

Summer 2007

Microthruster Experimental Analysis

Amy Denise Richards

Embry-Riddle Aeronautical University - Daytona Beach

Follow this and additional works at: <https://commons.erau.edu/db-theses>



Part of the [Aerospace Engineering Commons](#)

Scholarly Commons Citation

Richards, Amy Denise, "Microthruster Experimental Analysis" (2007). *Theses - Daytona Beach*. 174.
<https://commons.erau.edu/db-theses/174>

This thesis is brought to you for free and open access by Embry-Riddle Aeronautical University – Daytona Beach at ERAU Scholarly Commons. It has been accepted for inclusion in the Theses - Daytona Beach collection by an authorized administrator of ERAU Scholarly Commons. For more information, please contact commons@erau.edu.

MICROTHRUSTER EXPERIMENTAL ANALYSIS

By

Amy Denise Richards

A Thesis Submitted to the
Graduate Studies Office
in Partial Fulfillment of the Requirements for the Degree of
Master of Science in Aerospace Engineering

Embry-Riddle Aeronautical University

Daytona Beach, Florida

Summer 2007

UMI Number: EP32026

INFORMATION TO USERS

The quality of this reproduction is dependent upon the quality of the copy submitted. Broken or indistinct print, colored or poor quality illustrations and photographs, print bleed-through, substandard margins, and improper alignment can adversely affect reproduction.

In the unlikely event that the author did not send a complete manuscript and there are missing pages, these will be noted. Also, if unauthorized copyright material had to be removed, a note will indicate the deletion.

UMI[®]

UMI Microform EP32026
Copyright 2011 by ProQuest LLC
All rights reserved. This microform edition is protected against
unauthorized copying under Title 17, United States Code.

ProQuest LLC
789 East Eisenhower Parkway
P.O. Box 1346
Ann Arbor, MI 48106-1346

MICROTHRUSTER EXPERIMENTAL ANALYSIS

By

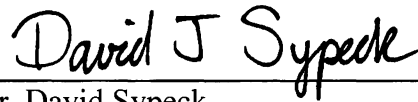
Amy Denise Richards

This thesis was prepared under the direction of the candidate's thesis committee chairmen, Dr. Reda Mankbadi and Dr. David J. Sypeck, Department of Aerospace Engineering, and has been approved by the members of her thesis committee. It was submitted to the Aerospace Engineering Department and was accepted in partial fulfillment of the requirements for the degree of Master of Science in Aerospace Engineering.

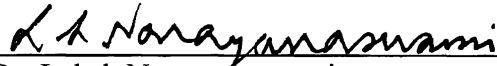
THESIS COMMITTEE:



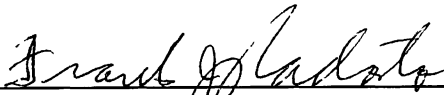
Dr. Reda Mankbadi
Chairman



Dr. David Sypeck
Chairman



Dr. Laksh Narayanaswami
Member



Dr. Frank Radosta
Acting Department Chair, Aerospace Engineering

6/14/07

Date



Dr. Christina Frederick
Vice President for Research

8/14/07

Date

ABSTRACT

Author: Amy Denise Richards
Title: Microthruster Experimental Analysis
Institution: Embry-Riddle Aeronautical University
Degree: Master of Science in Aerospace Engineering
Year: 2007

The purpose of this study was to design an experimental apparatus that could accurately test and measure the thrust efficiency of conical shaped microthrusters with varying divergence half angles. The experimental apparatus measured the thrust of micronozzles for various feed pressures in vacuum (to duplicate in space operation) as well as ambient. Calibration experiments confirmed the force measurement accuracy of the setup while gas thrust experiments were used to help determine the most efficient divergence half angle. Thrust results were compared to findings from two separate scientific studies that sought to optimize microthruster nozzles using CFD software.

TABLE OF CONTENTS

1 INTRODUCTION.....	1
<i>Nozzle Theory</i>	2
2 DESIGN.....	6
<i>Initial Design Considerations and Goals</i>	6
<i>Nozzle Angle Justification</i>	6
<i>Experimental Limitations</i>	7
<i>Nozzle Parameters</i>	7
<i>Propellant and Inlet Conditions</i>	8
3 EXPERIMENTAL.....	10
<i>Overall Measurement Setup</i>	10
<i>Vacuum Chamber and Pumping System</i>	11
<i>Nozzle Fabrication</i>	12
<i>Attachments and Setup</i>	13
<i>Data Acquisition Wire and Gas Hose Integration</i>	14
<i>Load Cell Calibration</i>	19
<i>Thrust Measurement Procedure</i>	20
4 TEST RESULTS.....	22
5 COMPUTATIONAL MODELS.....	25
6 DISCUSSION.....	31
<i>Results Analysis</i>	31
<i>Results Recap</i>	32
<i>Error Possibilities</i>	33
<i>Suggestions for Experimental Improvement</i>	34
<i>Summary</i>	34
REFERENCES.....	35
APPENDIX.....	36
<i>Appendix A: Thrust Versus Pressure For All Five Nozzles Fired At The Same Pressure (Vacuum Conditions)</i>	37
<i>Appendix B: Thrust Versus Pressure For Each Separate Nozzle Fired At Each Pressure (Vacuum Conditions)</i>	42
<i>Appendix C: Thrust Versus Pressure For All Five Nozzles Fired At The Same Pressure (Atmospheric Conditions)</i>	47

Appendix D: Thrust Versus Pressure For Each Separate Nozzle Fired At Each Pressure (Atmospheric Conditions)..... 52

LIST OF TABLES

Table 1. Study comparison information.	2
Table 2. Propellant and inlet parameter comparison.	8
Table 3. Load cell calibration data.	19
Table 4. Thrust measured for each nozzle at each feed pressure.	23
Table 5. Parameters used for the 1-D thrust calculation.	27
Table 6. Results recap.	32

LIST OF FIGURES

Figure 1. Typical convergent-divergent nozzle contour and parameters.	3
Figure 2. Conical and bell-shaped nozzle contours.....	7
Figure 3. Schematic of the overall measurement setup.	11
Figure 4. Vacuum chamber and pumping system.	12
Figure 5. Conical nozzle and connection details.....	13
Figure 6. Nozzle attachments and load cell setup.	14
Figure 7. Nozzle inside vacuum chamber (front view).	17
Figure 8. Nozzle inside vacuum chamber (side view).	17
Figure 9. Vacuum pumping system and a typical ion gauge reading during testing (4.7×10^{-5} Torr).....	18
Figure 10. Vacuum chamber and propellant feed system.....	18
Figure 11. Percent error between actual and measured force values.	20
Figure 12. Typical thrust vs. time data.	22
Figure 13. Plot of thrust measured for each nozzle at each total inlet pressure.....	24

1 INTRODUCTION

With the vast number of different spacecraft and space related technologies entering orbit around Earth, there is an increasing need for accurate and precise spacecraft control. Microthrusters are used for various applications on these spacecraft within the Earth's atmosphere and in space [1]. Microthrusters are exactly what the name implies, very small. It is appropriate to look at the microthruster system as a scaled down version of the larger system. The system is chosen based on mission requirements (size/weight of the spacecraft and impulse needed). Microthrusters are generally used in spacecraft that require small amounts of thrust, and their type can vary from electric to cold gas. Cold gas microthrusters are simply a system that contains a pressurized cold gas (monopropellant) and a nozzle. The gas is controlled by a valve system that can be a basic ball valve or an electronic solenoid valve. The valve can let the gas into the nozzle for small fractions of a second for pulsing or longer periods for steady state burns depending on the use of the microthruster.

The use of microthrusters range from vectoring control on satellites to the Manned Maneuvering Units used during Extra Vehicular Activities. There are also plans for small thrusters to propel sophisticated devices to examine the exterior of the space shuttle and space station for possible damage [1]. With these applications, there is a need for experimental means to accurately test micro-scaled propulsion systems before they are sent into space.

Nozzle contour optimization is a technique that promises to improve microthruster performance. Simulation methods such as Computational Fluid Dynamics (CFD) have been the most common method used for nozzle optimization. Accurate physical testing of different nozzles is needed to provide comparison data for these simulations. However, experimental testing methods are difficult to develop, and need very precise instrumentation along with accurate data gathering due to the very small amount of thrust developed by microthrusters. However, with this capability, actual working hardware can be improved and this is the next step toward effective space operation.

The goal of this project was to develop the experimental means to accurately measure small amounts of thrust and compare measured data to simulations. A literature search uncovered two sets of researchers who conducted studies using CFD modeling to simulate micronozzle performance. The two papers used as reference for this project are based on work independently done by researchers at the National Aeronautics and Space Administration (NASA) and Old Dominion University (ODU) [2, 3]. The NASA paper is titled “Investigation of Low-Reynold’s-Number Rocket Nozzle Design Using PNS-Based Optimization Procedure” by M.M. Hussaini and J.J. Korte [2]. The ODU paper is titled “NOZ-OP-2D: A CFD Based Optimization System For Axially Symmetric Rocket Nozzles” by J.P. Shebalin and S.N. Tiwari [3]. A brief discussion of the work done by these researchers is presented in later sections. Some particulars of the work by the two teams are shown in Table 1. Also shown are corresponding particulars for the work described here.

Study	Analysis Type	Nozzle Shape	Divergence Half Angle Range	Favored Divergence Half Angle
NASA, Hussaini and Korte [2]	CFD	Conical	20° - 30°	25.96°
ODU, Shebalin and Tiwari [3]	CFD	Conical	20° 30°	26.016°
ERAU, Present Study	Experimental	Conical	20°, 23°, 26°, 28°, 30°	26°

Table 1. Study comparison information.

Nozzle Theory

The purpose of a convergent-divergent nozzle is to expand a propellant gas as it exits the divergent portion of the nozzle and efficiently convert the available energy into thrust. The majority of the thrust is developed by accelerating the propellant gas (to sonic velocities at the nozzle throat) with the rest produced from the divergent section of the cone, Fig. 1. Therefore, the nozzle must be designed to smoothly accelerate the gas to produce the desired thrust.

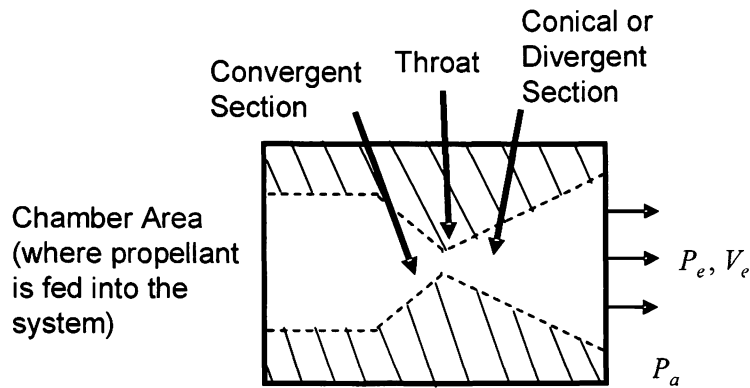


Figure 1. Typical convergent-divergent nozzle contour and parameters.

There are primarily three sections of the convergent-divergent nozzle shown above; the converging section, the throat, and the diverging section. In Fig 1., P_a is the ambient pressure, P_e is the exit pressure of the propellant, and V_e is the exit velocity of the propellant. The convergent section accelerates subsonic flow from the chamber while decreasing the gas pressure, and therefore increasing the kinetic energy of the gas. The throat section produces transonic flow, which is ideally equal to Mach 1 (choked). The sonic condition can only occur if the critical pressure is reached at the throat. The critical pressure is the pressure at the throat which gives a maximum isentropic mass flow rate. The divergent section then increases the flow to supersonic velocity [4].

Changes in ambient pressure, which can occur while traveling upward in altitude, can cause over or under expansion of the nozzle. These non-ideal cases happen when the ambient pressure does not equal the gas pressure at the nozzle exit. The ideal nozzle has equal ambient and exit pressure. However, in near vacuum conditions, the ambient pressure is zero and the gas will ultimately have a higher pressure upon exit [4].

The total force, or thrust, when exit pressure equals ambient pressure can be calculated using;

$$T = \dot{m} V_e = \left(\frac{\dot{m}}{g_0} \right) V_e \quad (1)$$

Where;

T - Force or thrust

\dot{m} - Propellant mass flow rate

\dot{w} - Propellant weight flow rate

V_e - Propellant exit velocity

g_0 - Acceleration of gravity (9.8 m/s²)

For a steady operating propulsion system moving through a homogeneous atmosphere, the total thrust is calculated using;

$$T = \dot{m}V_e + (P_e - P_a)A_e \quad (2)$$

Where;

P_e - Exit pressure

P_a - Ambient pressure

A_e - Exit area

The convergent section of such a nozzle usually has an inlet half angle of between 30° and 60°. The entrance is often designed to minimize the length of the nozzle and erosion of the nozzle material that can occur at high pressures and flow rates. Flow erosion was not a major factor for the experiments performed in this study.

The throat section of the nozzle needs to provide a good, smooth transition to supersonic flow. For the throat to do this, it must be free of obstructions and protrusions. These can occur in the form of weld splatter, slag, or rough machining. They can cause the kinetic energy of the propellant to be converted into thermal energy. This effect may even keep a sonic condition from being established at the throat. Also, the throat should have a cross-section that is as circular and as short as possible. The smaller the length of the throat, the more ideal the conditions are for sonic flow.

The divergent section of the nozzle is normally either conical or contoured. Contoured nozzles axially turn the flow, reducing divergent losses and are shorter in length. Even though contoured nozzles do increase specific impulse, overall performance is not greatly affected. The study performed here will use conical nozzles due to ease of machining and lower cost. Conical nozzles are typically designed for the altitude at which they are to be used, and this usually affects the throat-to-exit length [4]. For this study, nozzle length is not an issue because of the small nature of microthrusters and the fact that they are designed to be used in near space conditions (vacuum).

Analysis of the convergent-divergent nozzle is commonly done through a quasi one-dimensional calculation to evaluate the initial design of the nozzle. Specific assumptions are used to simplify the fluid dynamics. The primary assumptions are as follows [4]:

- The flow is isentropic and one-dimensional
- The gas is homogeneous, completely in the gaseous phase, and obeys the perfect gas law
- The gas is compressible and ideal
- The gas reservoir pressure and temperature are constant and assumed at or near room temperature
- Shock waves or discontinuities do not exist in the gas flow
- The gas flow is steady, constant, and short term transient effects during starting/stopping are neglected
- Gas exhaust velocity is directed axially
- Gas velocity, temperature, pressure, and density are uniform over any cross section area perpendicular to the nozzle axis
- The gas establishes chemical equilibrium in the chamber and composition is steady throughout the nozzle

The theory and assumptions as stated above, are used later in this study in conjunction with other flow parameters to perform a one-dimensional calculation. The experiments utilized real nozzles. The one-dimensional calculation was performed to establish a range of expected thrust as well as determine the level of accuracy needed for the experimental setup and measurement devices.

2 DESIGN

Initial Design Considerations and Goals

Microthrusters have distinct characteristics making them unique when compared to larger thrusters. The most critical characteristics being a short nozzle length and lower Reynolds number, Eqn. 3, which both contribute to the nozzle flow remaining laminar. The divergence angle of the nozzle is of particular interest because this angle has the greatest effect on nozzle efficiency. One goal of this work and the two reference papers was to test a range of nozzle half angles to determine the most efficient design.

$$\text{Re} = \frac{\rho V l}{\mu} \quad (3)$$

Where;

ρ - Propellant density

V - Propellant velocity

μ - Propellant viscosity

l - Length (throat diameter)

Nozzle Angle Justification

The first consideration for the experimental part of this project was to decide on exactly which half angles for the conical nozzles were of most interest. Both of the reference papers used nozzle divergence half angles of between 20° and 30° for their optimization work. These studies showed that very close to 26° was the most efficient half angle for both conical and bell shaped nozzles. Using these results as a guideline, it was decided that nozzle half angles of 20°, 26°, and 30° would be the baseline choices. These cover the full range of the previous research with the 26° nozzle being the assumed best design. The NASA and ODU research used extremely small steps in the half angle optimization (forward difference method with a 0.0001° step size). This is much easier to do with computational power, but not feasible with physical experiments. Therefore it was

decided to use half angles that were spaced approximately evenly between the upper and lower limits with the assumed best design inclusive. The other two selected nozzle angles were 28° and 23° , respectively. The nozzles would all be conical designs, leaving the testing of bell shaped nozzles as a possibility for others. Contours for typical conical and bell-shaped nozzles are shown below, Fig. 2.

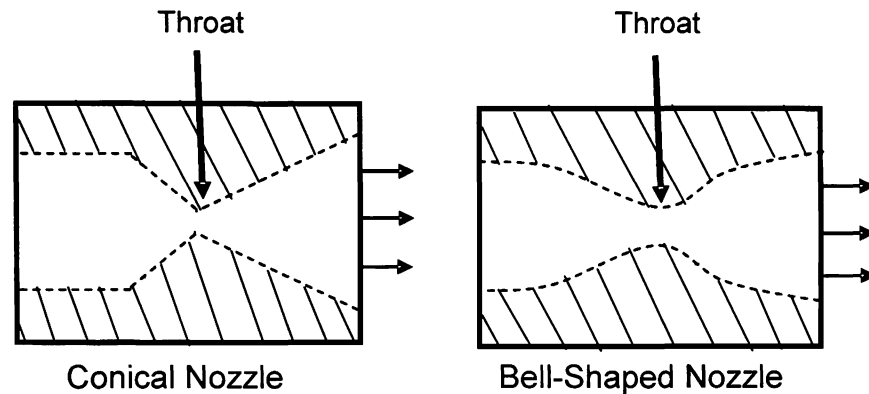


Figure 2. Conical and bell-shaped nozzle contours.

Experimental Limitations

For reasonable comparison to the published results, the nozzles for this experimental study had to be as close to simulation nozzles as possible. However, in the experimental arena, there are limitations imposed that are not apparent in the computational regime. Real world occurrences cause limitations in physical testing. These include cost, fabrication issues (which can impact design), specialized equipment needs, hazards (that can impact the environment and researchers), and the actual amount of time to test. Even with these limitations in place, the parameters were chosen to get as close as realistically possible to the parameters used by the reference papers.

Nozzle Parameters

In the reference papers, the area ratio was chosen as a fixed value for computational simulation. The area ratio is a function of the exit diameter, D_e , and throat diameter, D_t , of the nozzle;

$$AR = \left(\frac{D_e}{D_t} \right)^2 \quad (4)$$

Therefore, the area ratio for the present experiments had to be close to that of the reference papers. The nozzles for this study were chosen to have an exit area of 6.35 mm and a throat diameter of 0.762 mm resulting in an area ratio of 69. These parameters are similar to that reported in the reference papers [2, 3].

Propellant and Inlet Conditions

Additional design parameters used for this study compared to those of the reference papers are shown in Table 2, where P_0 and T_0 are the total inlet pressure and total inlet temperature of the propellant gas. The type of gas, along with its inlet pressure and temperature are significant because they, along with the throat diameter, influence the Reynolds number. This in turn affects whether the flow stays laminar or becomes turbulent.

Study	Propellant	Inlet Pressure (Pa)	Inlet Temperature (K)
NASA, Hussaini and Korte [2]	Hydrogen	150,000	1500
ODU, Shebalin and Tiwari [3]	Nitrogen	474	300
ERAU, Present Study	Nitrogen	200,000 to 600,000	300

Table 2. Propellant and inlet parameter comparison.

The two reference papers used differing gases for their simulations. The type of gas is important because density and viscosity of a particular gas affect the Reynolds number, and therefore, the flow nature of the gas. The study done at NASA used Hydrogen while the study done at ODU used Nitrogen. The present study chose Nitrogen because it was readily available and safer than Hydrogen.

The inlet pressures used for the NASA and ODU studies were 150,000 Pa and 474 Pa, respectively. The inlet pressure range of 200,000 to 600,000 Pa for the present study was driven by the experimental setup to be discussed later. The inlet temperatures used for the NASA and ODU studies were 1500 K and 300 K, respectively. The inlet temperature used for the present study was chosen to be 300 K, which is approximately room temperature. This choice avoids difficulties involved with accurately heating the gas to another desired temperature as well as hardware selection issues.

3 EXPERIMENTAL

Overall Measurement Setup

To measure small amounts of thrust, an experimental setup had to be designed and constructed. This apparatus had to be able to accurately determine the small amount of thrust produced by the micronozzles. A simple thrust stand would not work due to the potentially large amount of vibrations and torque created on the arm. The strain gauges used to measure deflection in the arm during thrusting would not likely be able to accurately read the small magnitude of force. Also, a data acquisition system would have to be purchased and connected to the strain gauges. Adequate calibration of this system could be difficult and not guaranteed. After evaluating several options, including a pendulum system, equipment from Instron Corporation (Norwood, MA) that was already available in the Materials Testing Lab at ERAU was chosen. The machine was an Instron 8802 materials test system with 8800 Fast Track control and acquisition. It was already setup to measure very large amounts of force utilizing a large capacity load cell for measurement. This machine had a data acquisition system installed and calibrated to the system. A small load cell (Instron model 2530-439 rated $\pm 5\text{N}$) could be purchased and attached to the system for measuring small forces. This system is easily calibrated, user friendly, and proved to be the best option available. Along with the new, much smaller capacity load cell, additional equipment would be needed such as valves, pressure gauges, gas supply tanks, feed tubing, a vacuum chamber, and attachments. This additional equipment was used to connect the nozzles to the load cell, provide Nitrogen propellant to the nozzles, regulate the pressure of gas going into the nozzles, and provide ambient vacuum conditions. A schematic of the measurement setup is shown in Fig. 3.

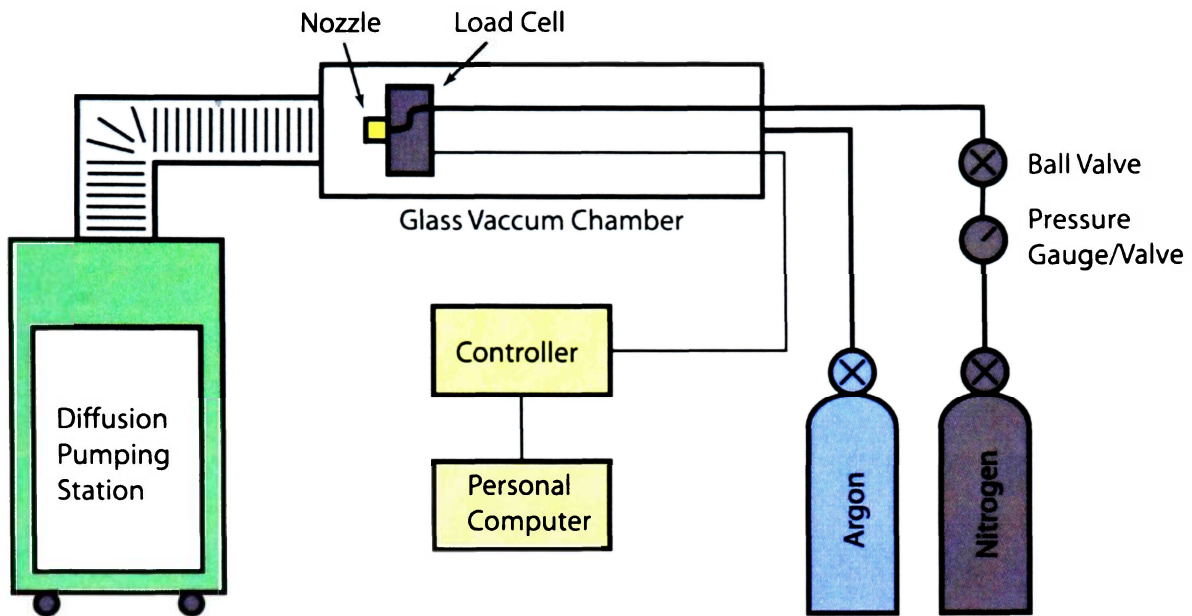


Figure 3. Schematic of the overall measurement setup.

Vacuum Chamber and Pumping System

Microthrusters are primarily used at the outer edge of the atmosphere or completely in space. Therefore, one of the environments needed for testing was vacuum. The vacuum chamber and diffusion pumping system is shown in Fig. 4. It provided a testing environment in which there was virtually no ambient pressure. The pumping system was made by Key High Vacuum Products (Nesconset, NY). The two reference papers used perfect vacuums for their simulations so this environment was also desirable for results comparison. The chamber itself was made from 150 mm ID quartz tubing and was connected to the pumping system via stainless steel tubing. Viton o-rings and vacuum grease were used for sealing. Pressure readings were measured using an ion gauge. For accurate pressure readings and a quality vacuum, the vacuum chamber was periodically purged with Argon gas during pump down. Argon gas purging helps force out unwanted particles (i.e., H₂O vapor, dust, other gases, etc.) that may reside within the chamber. Once the chamber pressure had reached a level in the range of 10^{-5} Torr or better, the experiments were run.

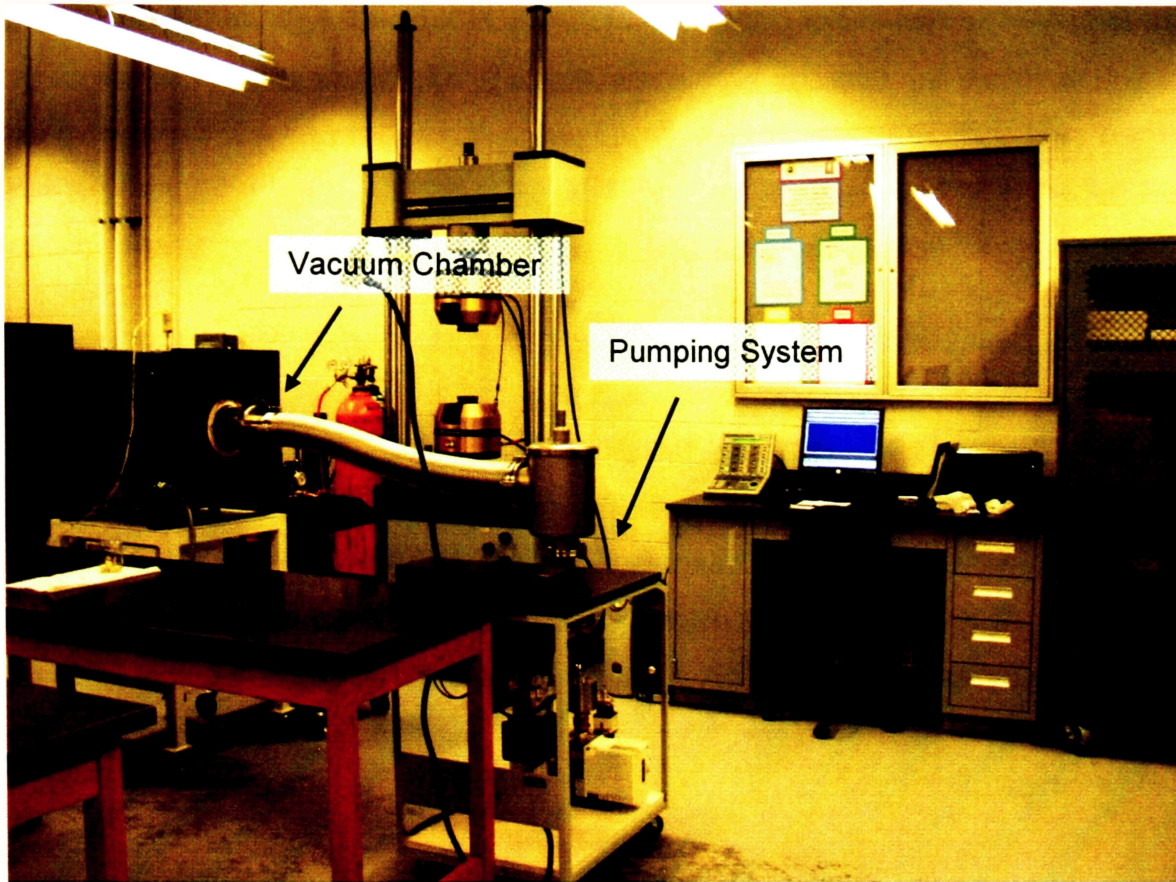


Figure 4. Vacuum chamber and pumping system.

Nozzle Fabrication

The nozzles for this study were originally chosen to be fabricated from a plastic; Polyetheretherketon (PEEK), because of availability and a softness that seemed to allow for easy fabrication. However, the nozzles machined from PEEK deformed during the machining process and produced significant flaws on the throat area surface. A smooth surface is necessary to prevent deviations in airflow that can create turbulence, decrease efficiency, and give poor results.

After having a little hindrance with the material selection, a much better material was ultra-machinable brass (alloy 360). It was soft enough for easy machining but hard enough to yield a smooth surface. For this round of fabrication, precaution was taken to ensure the throat was made properly so as to produce a sonic condition. Also, Standard English measurements were decided upon for machining to make drill selection easier. If

the correct drill bit sizes were not available, special tooling would have to be fabricated, which would be more costly. All of the nozzles had the chamber and the throat drilled using the same size drill bit such that, ideally, the only variance from nozzle to nozzle was the divergence angle. The threading and hose coupling entry (used at the back of the nozzle chamber to allow connection to the air hose) were also drilled similarly.

Nozzles were fabricated by Hudson Tool and Die Company (Ormond Beach, FL). The machinist used a high precision CNC lathe to shape out the nozzles. The stock material was 0.9525 cm (3/8 in) diameter ultra-machinable brass (alloy 360) rod. The nozzle chamber areas were tapped to accept a barbed hose coupling for Nitrogen gas inflow, Fig. 5. This chamber directed the flow into the throat area to help produce a sonic condition. Extra precaution was taken for this round of fabrication to ensure that the throat had potential to produce a sonic condition. The hose couplings were designed to accept 3.2 mm (0.125 in) ID gas feed tubing.

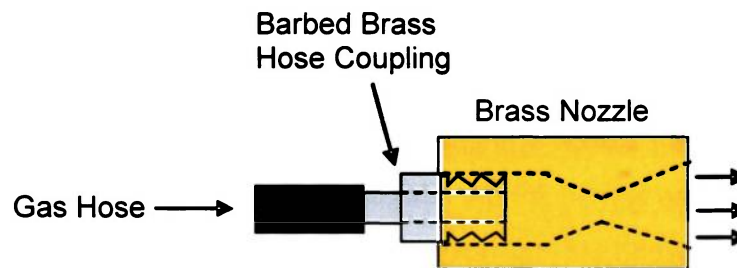


Figure 5. Conical nozzle and connection details.

Attachments and Setup

The nozzle attachment device was designed and fabricated from aluminum to mate the nozzles to the load cell, Fig. 6. This attachment contained tiny setscrews to hold the nozzle firmly in place as well as in line with the load cell. Good alignment is important to get an accurate reading of the thrust produced by the nozzles. Another attachment (the load cell steadying device) was fabricated to fit securely around the load cell and hold the load cell in place during testing. This attachment provided a solid anchoring surface during testing since movement by the load cell would affect the readings.

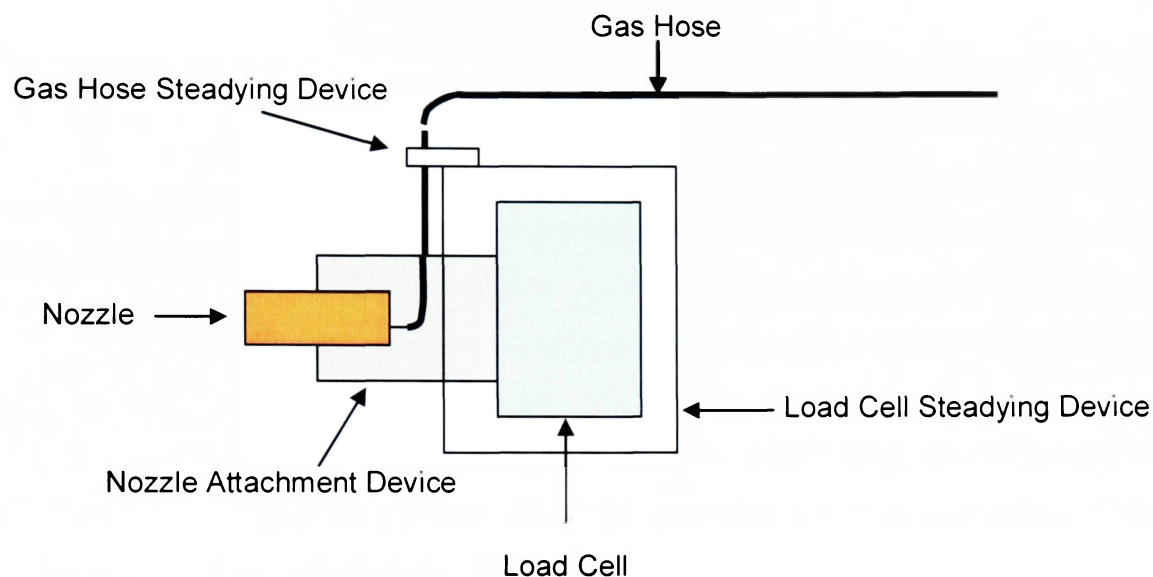


Figure 6. Nozzle attachments and load cell setup.

Data Acquisition Wire and Gas Hose Integration

Setting up the vacuum chamber correctly is very important and should be done meticulously to ensure accurate readings. The vacuum chamber had small orifices that allowed wires or hoses to be fed into the chamber. Shrink tubing was placed around the data acquisition wires to secure them. The wires and gas feed hose were then fed into separate stainless steel tubes, one for the gas hose and one for the load cell wires. These tubes were then filled with vacuum chamber epoxy to create an airtight seal inside each tube. The stainless steel tubes were chosen to fit tightly in the chamber orifices with sealing via Viton o-rings and vacuum grease.

Vacuum Chamber Preparation

Everything must be cleaned before entering the vacuum chamber. This is to prevent free particles from contaminating the chamber that can impair the achievable vacuum level and cause inaccurate reading of pressure inside the chamber. Methanol and laboratory wipes were used to wipe down all pieces of equipment going into the vacuum chamber.

Propellant Delivery

The Nitrogen gas propellant was delivered to the microthrusters using 3.2 mm (0.125 in) ID Viton tubing. Viton was chosen because its physical properties keep the material together under high vacuum and because its low partial pressure helps to minimize the number of potentially contaminating particles. Conventional rubber can break down when introduced into vacuum to introduce contaminating particles and undesired partial pressure. A gas hose was connected to the Nitrogen tank using a regulator/gauge which controlled the pressure at which Nitrogen was initially introduced into the hose. The hose was then run into a pressure gauge, followed by a ball valve, and lastly into the chamber, Fig. 3. Inside the chamber, the Viton hose passed through a steadying device placed onto the load cell steadying device, Fig. 6.

Experimental Apparatus Summary

- Instron Test System
 - Load cell measures thrust to ± 5 N with a $\pm 0.5\%$ error down to 1% of maximum load
 - Sensitivity at desired level
 - User friendly data acquisition system (5 kHz sampling rate)

- Vacuum Chamber
 - Provides a testing environment that closely approximates space conditions
 - 10^{-5} Torr or better vacuum level

- Load Cell Steadying Device
 - Used to stabilize the load cell
 - Fixed the load cell to minimize sliding and turning when applying thrust
 - Minimized torque on the load cell

- Nozzle Attachment Device
 - Fabricated from aluminum
 - Designed to allow for easy changing of thrusters

- Designed to allow gas hose connection to the back of thrusters without load cell centering offset
- Gas Hose
 - Viton material
 - Particles not likely to contaminate vacuum or feed gas
 - Connected to the nozzle using a 3.2 mm (0.125 in) barbed hose coupling
- Argon Gas
 - Allows purging of the vacuum chamber which flushes away contaminating particles
- Nitrogen Gas
 - Low density
 - Obtains a relatively low Reynold's number (high viscous effects)
 - Same gas that was used in the study by Shebalin and Tiwari from ODU
 - Has similar properties to Hydrogen gas that was used in the study by Hussaini and Korte from NASA
- Control Valve and Gauge
 - Regulates the feed pressure of Nitrogen gas into the nozzle
 - Quick firing ball valve

Additional photographs of the experimental devices can be seen in Figs. 7 - 10.

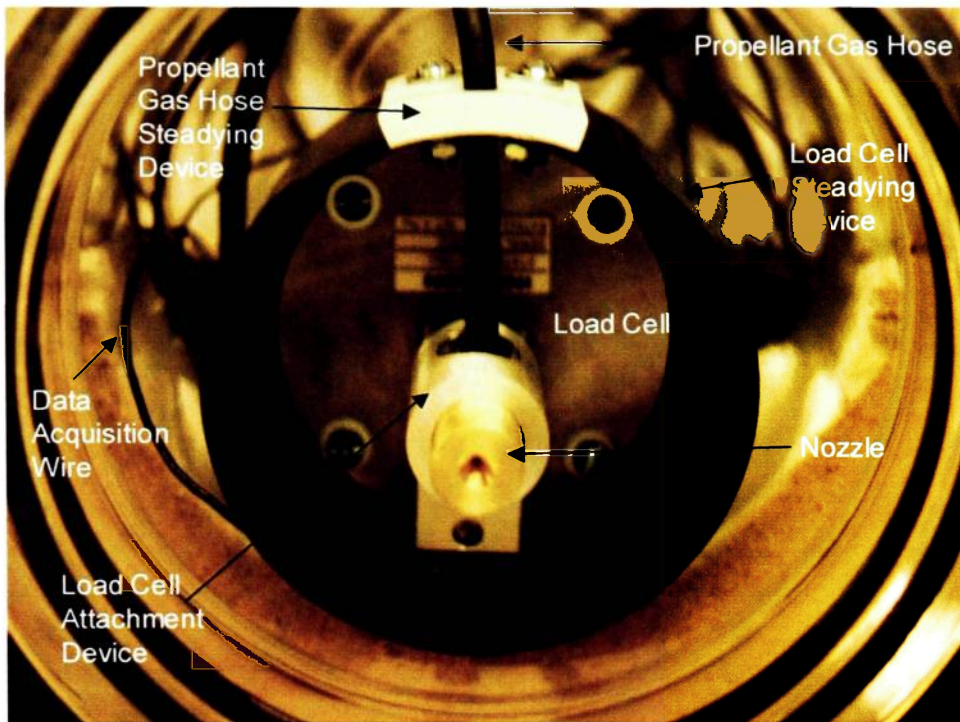


Figure 7. Nozzle inside vacuum chamber (front view).

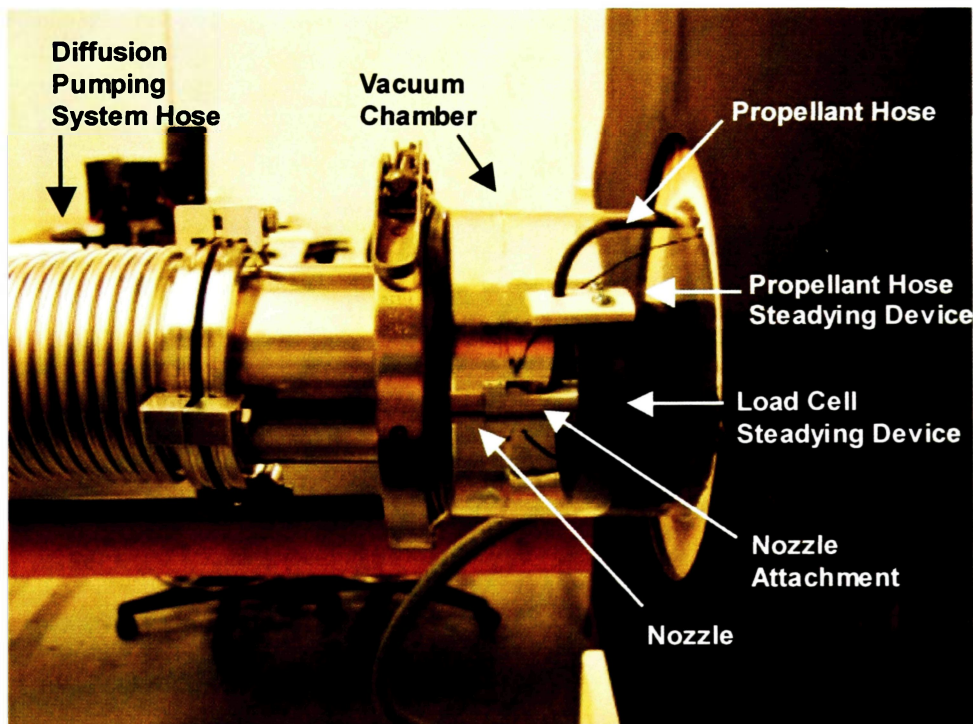


Figure 8. Nozzle inside vacuum chamber (side view).

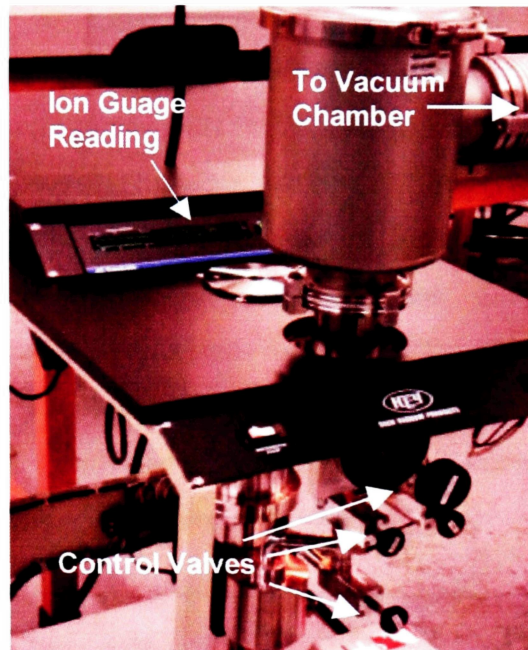


Figure 9. Vacuum pumping system and a typical ion gauge reading during testing (4.7×10^{-5} Torr).

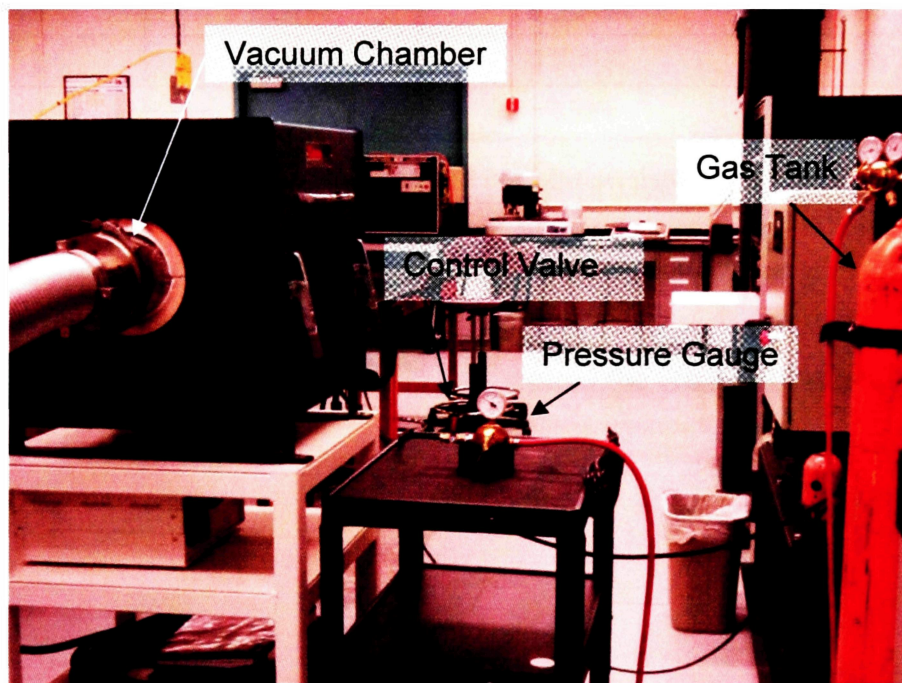


Figure 10. Vacuum chamber and propellant feed system.

Load Cell Calibration

The load cell used in this study measures thrust to ± 5 N with a $\pm 0.5\%$ error down to 1% of the maximum load. Calibration of the Instron machine and load cell was performed to verify the accuracy of readings obtained by the data acquisition system. The calibration involved taking ASTM Class 1 calibration masses (Troemner, Thorofare, NJ) from 0.1 to 100 grams and placing them one at a time on the load cell (vertically oriented). An average force reading was taken for each separate mass. Sampling occurred at 5 kHz. The calibration masses were purchased specifically for this study along with their calibration certificates. The actual force that should be read by the data acquisition system was calculated for each mass. Table 3 shows a comparison of the actual and measured force values along with percent measurement error.

Calibration Mass (g)	Actual Force (N)	Measured Force (N)	Measurement Error (%)
0.01	0.0000981	0.000133	35
0.10	0.000981	0.00118	20
0.50	0.00491	0.00494	0.82
1.0	0.00981	0.00982	0.18
100	0.981	0.981	0.045

Table 3. Load cell calibration data.

The percent error between actual and measured values is plotted in Fig. 11. The amount of thrust produced by nozzles utilized in this study is expected to fall in the region between the 1 and 100 gram masses. In that region, the error is between 0.045% and 0.18%.

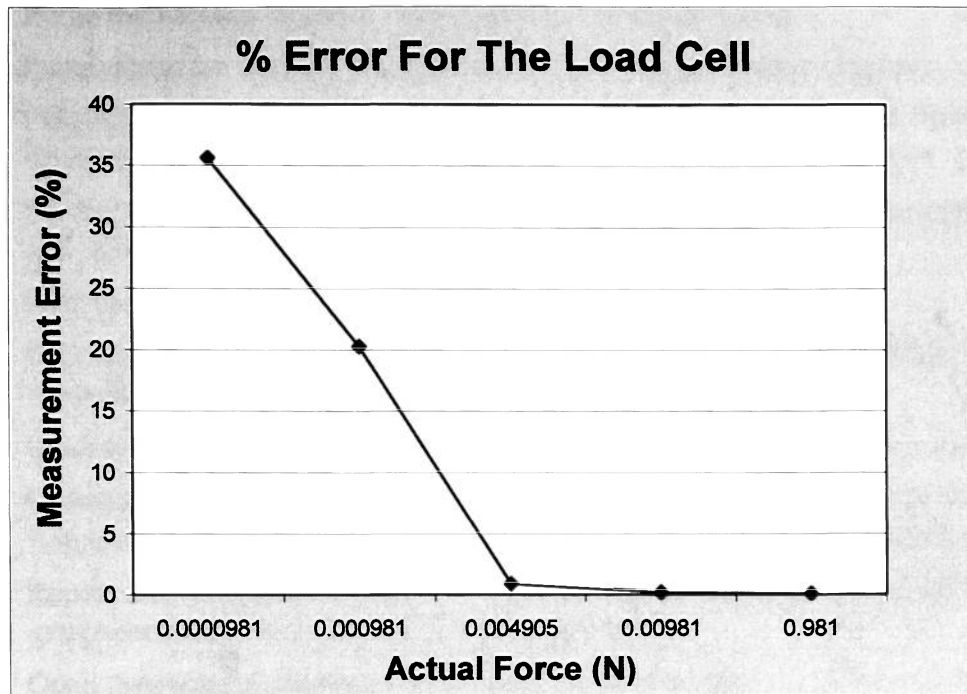


Figure 11. Percent error between actual and measured force values.

Thrust Measurement Procedure

The testing procedure was as follows:

1. Feed the gas supply hose and wires through the orifices and into the vacuum chamber
2. The load cell should be mounted on the load cell steadying device via the mounting screws
3. Insert the load cell and steadying device into the vacuum chamber
4. Attach the nozzle attachment device onto the load cell via setscrews
5. Feed the gas hose through the hose steadying device, nozzle attachment device and onto the nozzle
6. Attach the nozzle onto the nozzle attachment device
7. Check the gas hose and wire locations to ensure that they are not in front of the thruster
8. Pressure in the gas tank regulator should be high enough so that the pressure of gas allowed into the system can be set accurately on the control valve
9. Set the gauge on the control valve to the desired level
10. Seal the vacuum chamber

11. Purge the vacuum chamber with Argon gas while pumping
12. Pump down the vacuum chamber to 10^{-5} Torr range or better (Figure)
13. Purging and pumping down the vacuum chamber should be done three or four times to ensure the vacuum pressure is in the 10^{-5} Torr range or better
14. Set the data acquisition system to the desired settings (i.e., data acquisition rate and ASCII file to which the data is saved)
15. Start the data acquisition program
16. Take data for five seconds before opening the control valve to obtain a reading for background noise and vibration
17. Quickly open the control valve to begin firing and leave open for ten seconds
18. Quickly close the control valve and leave the data acquisition system running for five more seconds (again for background noise and vibration measurement)
19. Repeat this procedure (Steps 11 - 20) for the next inlet pressure until all inlet gauge pressures¹ (0.1 through 0.5 MPa) are tested
20. Open the vacuum chamber and connect the next nozzle
21. Test each consecutive nozzle using the same procedure (Steps 5 - 20) as stated above

¹ The supply pressure gauge will read this pressure, however the actual absolute feed pressure is the gauge pressure plus atmospheric pressure. The difference in pressure is due to the fact that these gauges record pressure differential. When reading “gauge” pressure (that above atmospheric), absolute pressure is simply obtained by adding atmospheric pressure (0.1 MPa) to the gauge reading.

4 TEST RESULTS

During each test run, the data acquisition system recorded five thousand force values per second. This data was then plotted on graphs of Thrust (N) vs. Time (s), APPENDIX. The plots include a few seconds before and after the actual firing of the nozzle to give a baseline value for noise in the system. The noise is caused by vibrations from the vacuum chamber pumping system along with electrical noise. A typical plot is shown in Fig. 12 below. The plots show a sharp increase in thrust at the point when the valve is opened as gas begins to flow through the nozzle (true thrust found here). Thrust decreases over the next few seconds (due to pressure increasing in the vacuum chamber as the Nitrogen gas emitted from the nozzle permeates the chamber). A sharp decrease in thrust then occurs as the valve is closed and gas flow to the nozzle is stopped.

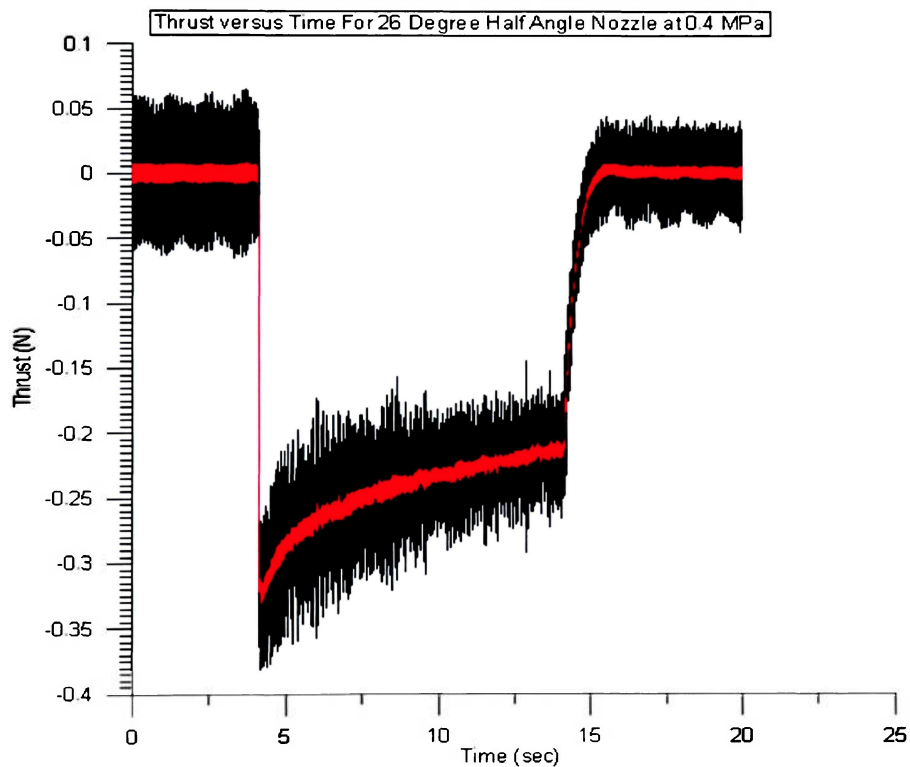


Figure 12. Typical thrust vs. time data.

Due to background noise captured by the load cell, the true thrust value must be extracted from the plot. True thrust is taken at the point where the valve is just opened and the gas has not been allowed to compromise the vacuum just yet. This value is read at the mean

of the plotted force data as shown in Fig. 12 (the red line is a 100 point moving average for smoothing). Note that the thrust values are negative due to the load cell reading in the negative direction (compression reads negative). The actual thrust is the positive counterpart (i.e., all numbers should be multiplied by negative one). Noise increases and decreases the thrust value both above and below the center of the data line; therefore the average of this data was used. After true thrust was measured, the average values of tests for each specific nozzle were taken and reported. Two tests were performed for each inlet pressure. Table 4 shows thrust results for each nozzle (half angles are indicated) with corresponding total inlet pressures. Fig. 13 shows a plot of the data. Individual test results for all nozzles over the range of inlet feed pressures can be found in the APPENDIX.

Total Inlet Pressure (MPa)	Thrust (N)				
	20°	23°	26°	28°	30°
0.2	0.0870	0.0841	0.0970	0.0931	0.0973
0.3	0.1509	0.1373	0.1603	0.1513	0.1545
0.4	0.2064	0.1850	0.2146	0.2040	0.2028
0.5	0.2580	0.2286	0.2688	0.2604	0.2547
0.6	0.3096	0.2795	0.3258	0.3152	0.3070

Table 4. Thrust measured for each nozzle at each feed pressure.

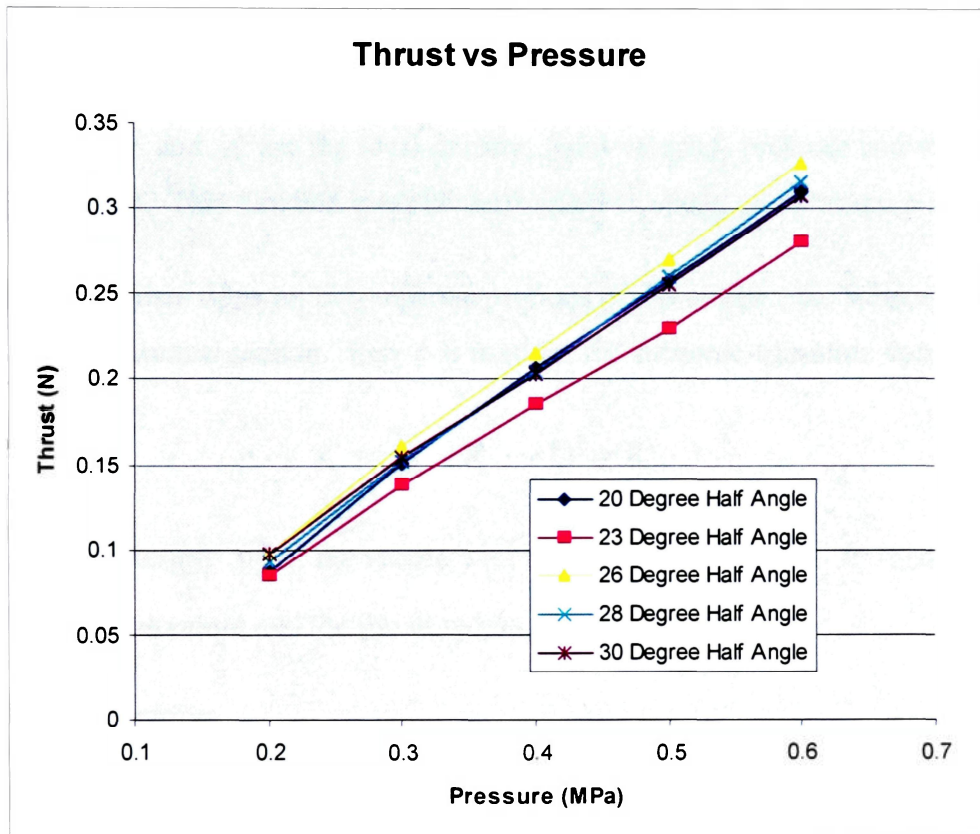


Figure 13. Plot of thrust measured for each nozzle at each total inlet pressure.

5 COMPUTATIONAL MODELS

Computational Calculation by Hussaini and Korte from NASA

This study [2] used an inlet pressure of 150,000 Pa and an inlet temperature of 1500 K. An objective function, Eqn. 5, is defined as the exit thrust into a vacuum dependent of set parameters;

$$Obj(X) = \int_0^{A_{exit}} (\rho u^2 + p) dA \quad (5)$$

Where ρ , u , p and A are the local density, axial velocity, pressure and cross-section area, respectively. This function must be maximized to obtain an optimum nozzle design.

Calculations are then done on two separate sections of the nozzle; the subsonic-transonic section, and the conical section. Eqn. 6 is used for the subsonic-transonic section;

$$x^2 + (y_w - R_c - r^*)^2 = R_c^2 \quad (6)$$

Where x is the length, y_w is the nozzle wall radius or height, while R_c and r^* are the throat radius of curvature and the throat radius, respectively.

For the conical section;

$$y_w = y_0 + \tan(\theta_c) \Delta x \quad (7)$$

Where θ_c is the cone angle and $\Delta x = x - x_0$ where x_0 and y_0 are the initial points for the conical section.

Upon optimization of these three equations using a CFD program, a divergence half angle of 25.96° was found to be the most efficient [2].

Computational Calculation by Shebalin and Tiwari from ODU

For this study [3], the inlet pressure and temperature were 474 Pa and 300 K, respectively. The specific impulse was chosen to be the objective function for this calculation.

The wall contour of the nozzle for this study is found using;

$$r(x) = r_t + R_{curve} - \sqrt{R_{curve}^2 - x^2} \quad (x_{in} \leq x \leq x_{inl}) \quad (8)$$

where R_{curve} is the radius of curvature of the nozzle at the throat and is found using Eqn. 9. Definitions for other variables are found in [3].

$$R_{curve} = \left(\frac{R_{curve}}{r_t} \right) r_t \quad (9)$$

The contour of the supersonic region is obtained by;

$$r_{inl} = r(x_{inl}) = A + Bx_{inl} \quad (10)$$

$$r_{exit} = r(x_{exit}) = A + Bx_{exit} \quad (11)$$

Where $x_{inl} < x \leq x_{exit}$ and the coefficients A and B are from the geometry parameters given by the (x, y) coordinates of the endpoints.

Solving Eqns. 10 and 11 simultaneously results in;

$$A = r_{inl} - x_{inl} \left(\frac{r_{exit} - r_{inl}}{x_{exit} - x_{inl}} \right) \quad (12)$$

$$B = \frac{r_{exit} - r_{inl}}{x_{exit} - x_{inl}} \quad (13)$$

Combining Eqns. 12 and 13 results in Eqn. 14 which is used to find the contour of the conical section as a function of known nozzle dimensions;

$$r(x) = r_{inf l} + (x - x_{inf l}) \frac{r_{exit} - r_{inf l}}{x_{exit} - x_{inf l}} \quad (x_{inf l} < x \leq x_{exit}) \quad (14)$$

The above sequence was incorporated into a grid generation program and then a computational fluid dynamics routine (VULCAN) for optimization. The results lead to a divergence half angle of 26.016° as the best [3].

One-Dimensional Calculation for This Study at ERAU

A one-dimensional calculation was performed for the 26° half angle nozzle using the parameters shown in Table 5. These calculations predicted thrust to be approximately 0.397 N. This thrust value does not take into account losses.

Parameter	Abbreviation	Value	Units
Throat diameter	D_t	7.62×10^{-4}	m
Exit diameter	D_e	6.35×10^{-3}	m
Gas constant	R	296.93	J/kg-K
Specific heat ratio	γ	1.4	
Acceleration of gravity	g	9.81	m/s^2
Ambient pressure	P_{amb}	0	MPa
Inlet pressure	P_{in}	0.5	MPa
Inlet temperature	T_{in}	300	K

Table 5. Parameters used for the 1-D thrust calculation.

Calculation Steps

The following equations were used to carry out the one-dimensional calculation [4]. Subscripts t and e represent the throat and exit regions while M is the Mach number. Other variable are defined periodically within this document.

Inlet pressure divided by throat pressure gives the ratio ($M_t = 1$ at the throat);

$$\frac{P_m}{P_t} = \left[1 + \left(\frac{\gamma - 1}{2} \right) M_t^2 \right]^{\frac{\gamma}{\gamma - 1}} = 1.893 \quad (15)$$

Throat pressure can now be obtained by;

$$P_t = P_m \left(\frac{P_t}{P_m} \right) = 264100 \text{ Pa} \quad (16)$$

Inlet temperature divided by throat temperature gives the ratio;

$$\frac{T_m}{T_t} = 1 + \left(\frac{\gamma - 1}{2} \right) M_t^2 = 1.200 \quad (17)$$

Throat temperature can now be obtained by;

$$T_t = T_m \left(\frac{T_t}{T_m} \right) = 250 \text{ K} \quad (18)$$

Density of the gas at the throat is found using throat pressure and temperature;

$$\rho_t = \frac{P_t}{RT_t} = 3.558 \text{ kg/m}^3 \quad (19)$$

Speed of sound at the throat is found using throat temperature;

$$a_t = \sqrt{\gamma RT_t} = 322.4 \text{ m/s} \quad (20)$$

Assuming $M_t = 1$ at the throat, the velocity of the gas can be obtained by;

$$V_t = a_t M_t = 322.4 \text{ m/s} \quad (21)$$

The Sutherland Equation accounts for the effect of temperature upon viscosity;

$$\mu_N = \mu_{0N} \left(\frac{T_t}{273} \right)^{\frac{2}{3}} \left(\frac{273 + S_N}{T_t + S_N} \right) = 1.55 \times 10^{-5} \text{ kg/m-s} \quad (22)$$

Where $\mu_{0N} = 1.66 \times 10^{-5} \text{ kg/m-s}$ and $S_N = 106.7 \text{ K}$ for Nitrogen [5].

The following equations can also be found in [5]:

Reynolds number is found using;

$$\text{Re} = \frac{\rho_t V_t D_t}{\mu_N} = 56,390 \quad (23)$$

Exit temperature is found using;

$$T_e = T_m \frac{T_e}{T_m} = 300 \frac{1}{9.794} = 30.63 \text{ K} \quad (24)$$

Exit pressure is found using;

$$P_e = P_m \frac{P_e}{P_m} = 500000 \frac{1}{2942} = 170.0 \text{ Pa} \quad (25)$$

Density at the exit is found using;

$$\rho_e = \frac{P_e}{RT_e} = 0.01869 \text{ kg/m}^3 \quad (26)$$

Area at the throat is found using;

$$A_t = \frac{\pi D_t^2}{4} = 4.560 \times 10^{-7} \text{ m}^2 \quad (27)$$

Area at the exit is found using;

$$A_e = \frac{\pi D_e^2}{4} = 3.167 \times 10^{-5} \text{ m}^2 \quad (28)$$

Speed of sound at the exit is found using;

$$a_e = \sqrt{\gamma RT_e} = 112.8 \text{ m/s} \quad (29)$$

Exit velocity is found using;

$$V_e = a_e M_e = 112.8 (6.63) = 748.2 \text{ m/s} \quad (30)$$

Mass flow rate is found using;

$$\dot{m} = \rho V_t A_t = 5.230 \times 10^{-4} \text{ kg/s} \quad (31)$$

Thrust is found using;

$$T = \dot{m} V_e + (P_e - P_a) A_e = 0.397 \text{ N} \quad (32)$$

Thrust coefficient is found using;

$$c_f = \frac{T}{P_m A_t} = 1.740 \quad (33)$$

Specific impulse is found using;

$$Isp = \frac{T}{\dot{m} g} = 77.30 \text{ s} \quad (34)$$

The purpose of the 1-D calculation was to generate an approximate thrust value for the most efficient nozzle used in this study.

6 DISCUSSION

Results Analysis

The goal of this study was to develop a system by which micronozzles can be accurately tested as well as provide validation for computational simulations. The results (Fig. 13) of this study lie within the expected and acceptable range reported by the reference papers and the one-dimensional analysis. The requirements needed for nozzle setup and accurate measurement were also met for this study.

It is recognizable that thrust will rise with an increase in pressure being fed to the nozzle. However it is not as obvious what effect the divergence angle will have. The results obtained from the experiments show that the angle can have influence on thrust. Therefore it is important to test multiple nozzles to observe which angle yields the best performance. The results of this experiment indicate that the 26° nozzle provides thrust values better than all others tested. This agrees with the computational efforts of Hussaini and Korte from NASA as well as Shebalin and Tiwari from ODU.

The only data in Fig. 13 that cannot be conclusive is that which corresponds to 0.2 MPa feed pressure. This is because the entire set of data points lie closely together, which is why obtaining a range of data for different feed pressures is necessary. The most efficient angle must have higher thrust overall, and 26° fills this requirement. If looking at only the 28° and 30° nozzles, the 30° nozzle seems to be more efficient at lower pressures while the 28° degree nozzle is more efficient at higher pressures. The 20° nozzle is slightly less efficient than the 28°, however, it must be recognized that 28° is closest to the 26° degree nozzle. The 23° nozzle has lower thrust overall, and is therefore the weakest performing nozzle.

The reason for the 23° nozzle performing poorly is puzzling and could be partly due to experimental error. This might include; excess noise, human error when reading the data, or roughness in the nozzle due to machining. Please refer to the APPENDIX for a recap of Thrust vs. Pressure plots. The plots compare thrust produced by the nozzles at the different pressures used in the experiments. All of the plots show the same trends

discussed above, with the 26° nozzle producing the most thrust, and therefore being the most efficient angle.

The one-dimensional calculation performed earlier for a total feed pressure of 0.5 MPa gives a thrust value of 0.397 N while the highest thrust value obtained experimentally for the 26° degree nozzle at 0.5 MPa is 0.269 N. The calculated value is higher most likely because the equations use idealizations and assumptions that are not the case with the actual experiment. Also error, discussed in a later section, leads to losses in the thrust value. Observe that the one-dimensional calculations predict an exit temperature of 30.63 K which may be lower than the vaporization temperature of Nitrogen at low pressure. Hence, the calculations are viewed somewhat cautiously with need for further, more detailed investigation.

Results Recap

Thrust results for the two reference studies were obtained through CFD analysis while the results from this study were found through experimental evaluation. A results summary is shown below in Table 6. The study by Hussaini and Korte from NASA [2] obtained an optimum half angle of 25.96° for their conical nozzle. The study by Shebalin and Tiwari from ODU [3] obtained an optimum half angle of 26.016° . The present study at ERAU found a divergence half angle of 26° degrees to be the most efficient (even with higher Reynolds numbers than the reference studies).

Study	Reynolds Number	Favored Divergence Half Angle
NASA, Hussaini and Korte [2]	1624.46	25.96°
ODU, Shebalin and Tiwari [3]	357.57	26.016°
ERAU, Present Study	56,390 (for $P_0 = 0.5$ MPa)	26°

Table 6. Results recap.

Error Possibilities

Error is an expected part of any experiment and calculation. In this study, error can enter in several ways. First of all, there are possible slight variations in the nozzle geometry that can occur during fabrication. These variations can occur in throat length, how the nozzles are centered in the brass material, and roughness of the machined area. The throat length can lead to error because if it is too long, the flow may deviate from a true sonic condition. The throat area and diameter must also be consistent at all points along the length of the throat. How the nozzles are centered in the brass material is another factor that can be problematic. The nozzle contour was not machined around the outside of the nozzle, therefore, if the nozzle is not centered in the material, the force cannot act axially on the load cell. Machining of the extra material around the nozzle was not needed in this study because nozzle mass was not an issue (the material could be removed for actual use in space). Although brass can be machined to be very smooth, there is still the possibility of roughness on the machined surfaces.

A gauge and a control valve regulate the inlet pressure which is assumed to be absolutely accurate, however, as with any experiment or calculation, error exists. There also may be a small amount of error in reading the gauge, which is performed by an observer who views notches on a dial. Turning the valve to start and stop the firing may also deviate from the five and ten second mark. Simple rounding errors could have also occurred in the calculations.

The Instron machine is rated to ± 5 N with a $\pm 0.5\%$ error down to 1% of the maximum load. This was tested through calibration from the company as well as the calibration conducted in this study. This particular machine proved to be better than the rated accuracy, however there still exists a small amount of error in the measurement.

Even though it is not accounted for in this study, there must be some amount of head loss due to pipe bending and friction but this is believed to be small.

Suggestions for Experimental Improvement

Suggestions for further research include reducing known sources of error and testing over a broader range of parameters. Ways of accomplishing these goals include but are not limited to:

- Using a different range of divergence half angles and also testing bell-shaped nozzles
- Experimenting with different inlet temperatures
- Changing the placement/type of control valve (possibly closer to the nozzle and within the vacuum chamber)
- Additional sensors inside the vacuum chamber may provide information on exit pressure and temperature to assist calculations and analysis

Summary

This study focused upon an experimental apparatus that could accurately test and measure the thrust efficiency of conical shaped microthrusters with varying divergence half angles. The experimental apparatus measured the thrust of micronozzles for various feed pressures in vacuum (to duplicate in space operation) as well as ambient. Calibration experiments confirmed the force measurement accuracy of the setup while gas thrust experiments were used to help determine the most efficient divergence half angle. Thrust results were compared to findings from two separate scientific studies that sought to optimize microthruster nozzles using CFD software.

Thrust results from the two reference studies were obtained through CFD analysis while results from this study were found through experimental evaluation. The study by Hussaini and Korte from NASA [2] obtained an optimum half angle of 25.96° for their conical nozzle. The study by Shebalin and Tiwari from ODU [3] obtained an optimum half angle 26.016° . The present study at ERAU found a divergence half angle of 26° to be the most efficient (thrust as the baseline determining factor). As anticipated, a one-dimensional calculation predicted thrust to be larger than measured suggesting a need for further, more detailed comparison analysis.

REFERENCES

1. www.nasa.gov (2007).
2. M.M. Hussaini and J.J. Korte, “Investigation of Low-Reynolds-Number Rocket Nozzle Design Using PNS-Based Optimization Procedure”, NASA TM-110295 (1996).
3. J.P. Shebalin and S.N. Tiwari, “NOZ-OP-2D: A CFD-based Optimization System for Axially Symmetric Rocket Nozzles”, AIAA-2001-1062 (2001).
4. Fundamentals of Fluid Mechanics, 4th edition, B.R. Munson and D.F. Young et al., Wiley and Sons, New York (2002).
5. Rocket Propulsion Elements, 7th edition, G.P Sutton and O. Biblarz, Wiley and Sons, New York (2001).
6. Fundamentals of Fluid Mechanics, F.M. White, Wiley and Sons, New York (1999).

APPENDIX

The following pages contain plots that show thrust vs. time, recorded by the Instron data acquisition system. Note that thrust values are reported negative due to the load cell reading in the negative direction (compression direction). Thrust is actually the positive counterpart (i.e., all values should be multiplied by negative one). Data for experiments performed in ambient air are included for completeness where less noise is apparent owing to the lack of a vacuum pumping system.

Appendix A: Thrust Versus Pressure For All Five Nozzles Fired At The Same Pressure (Vacuum Conditions)

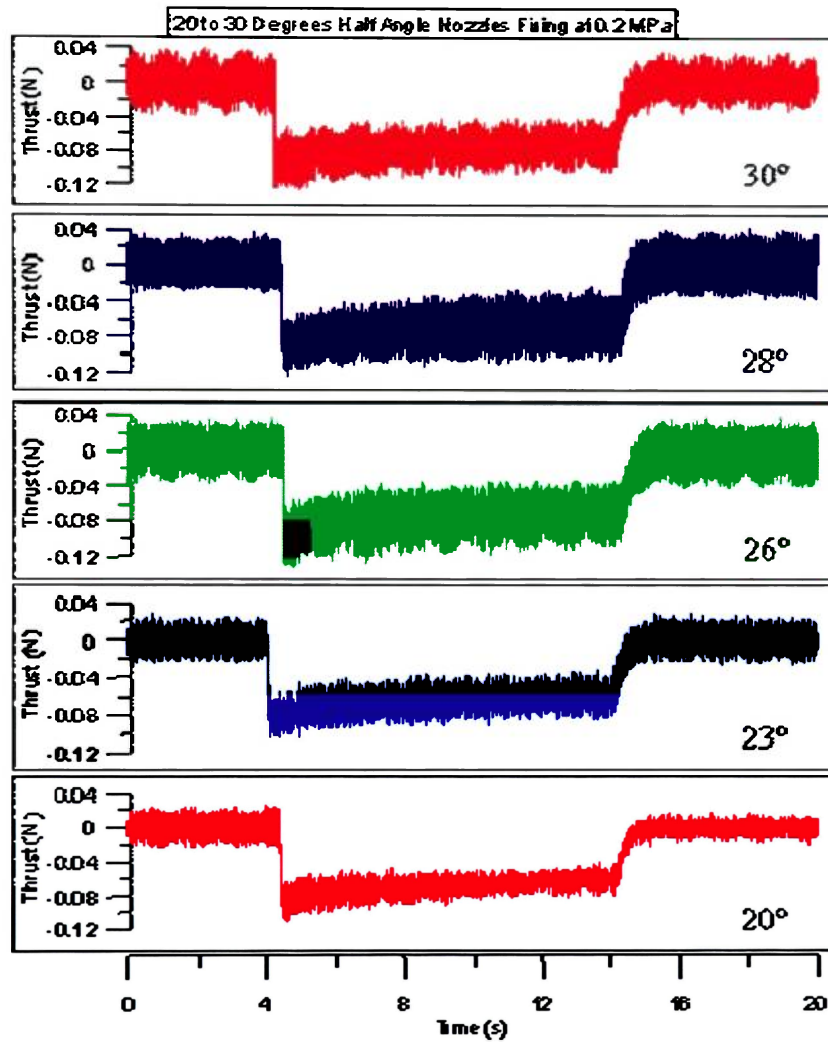


Figure A1. 20 to 30 degrees half angle nozzles firing at 0.2 MPa (vacuum).

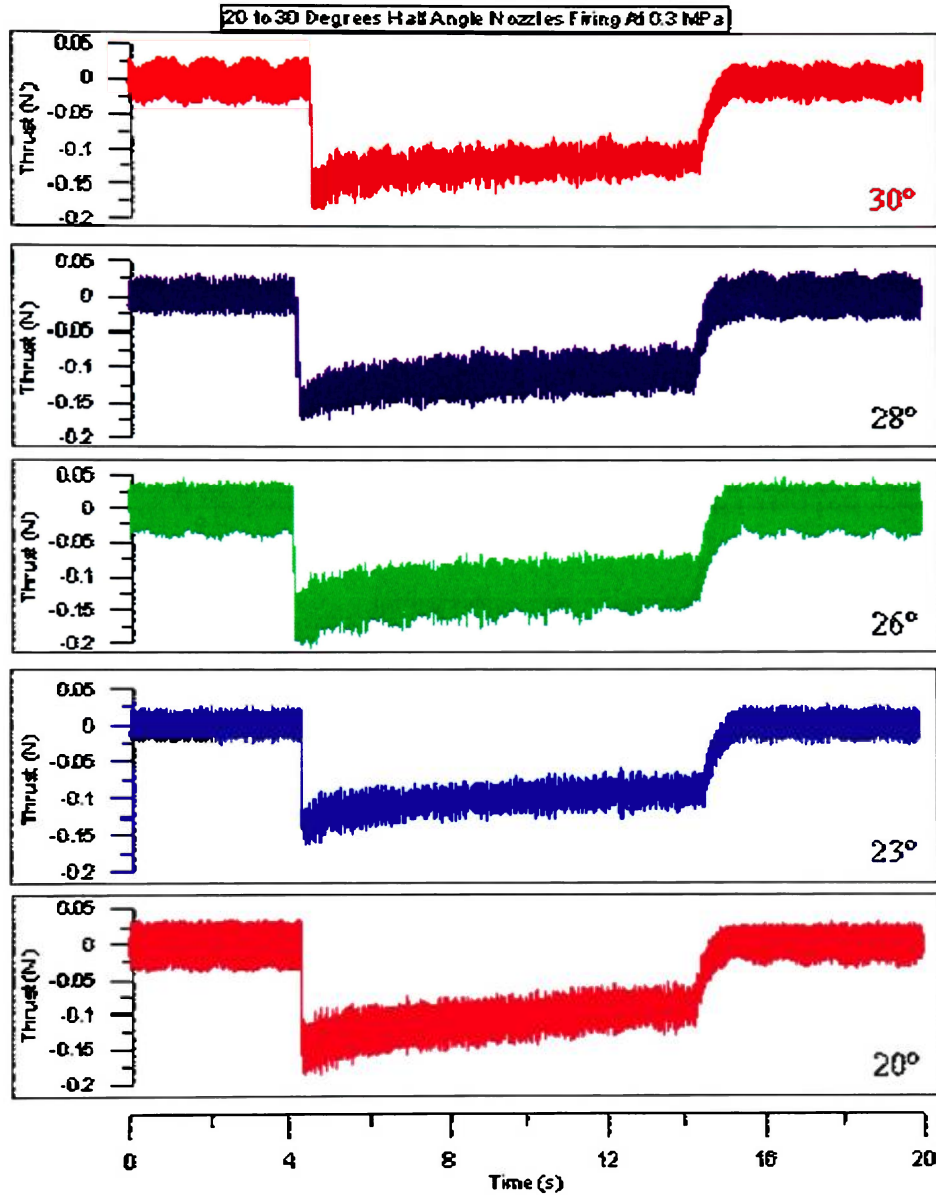


Figure A2. 20 to 30 degrees half angle nozzles firing at 0.3 MPa (vacuum).

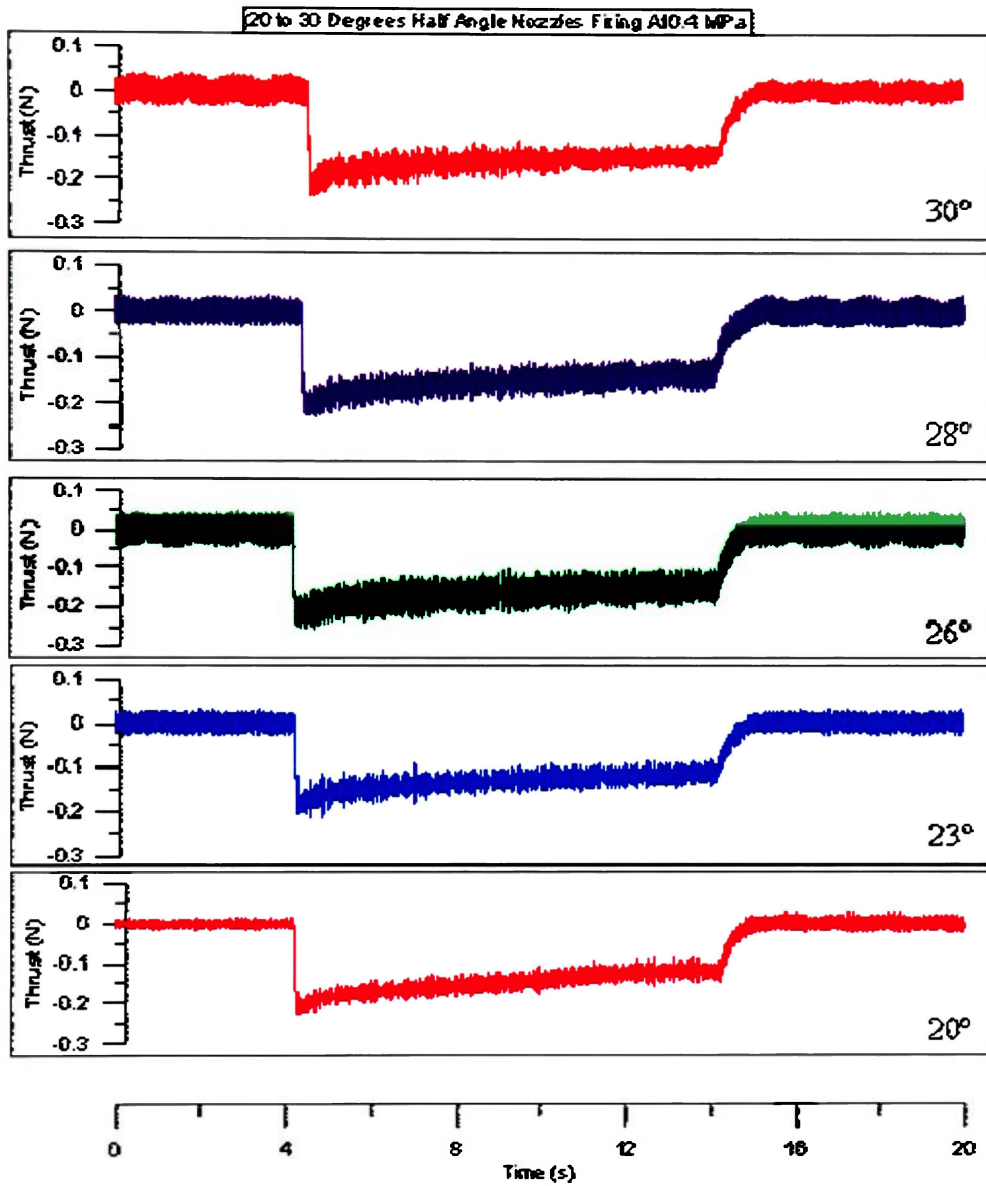


Figure A3. 20 to 30 degrees half angle nozzles firing at 0.4 MPa (vacuum).

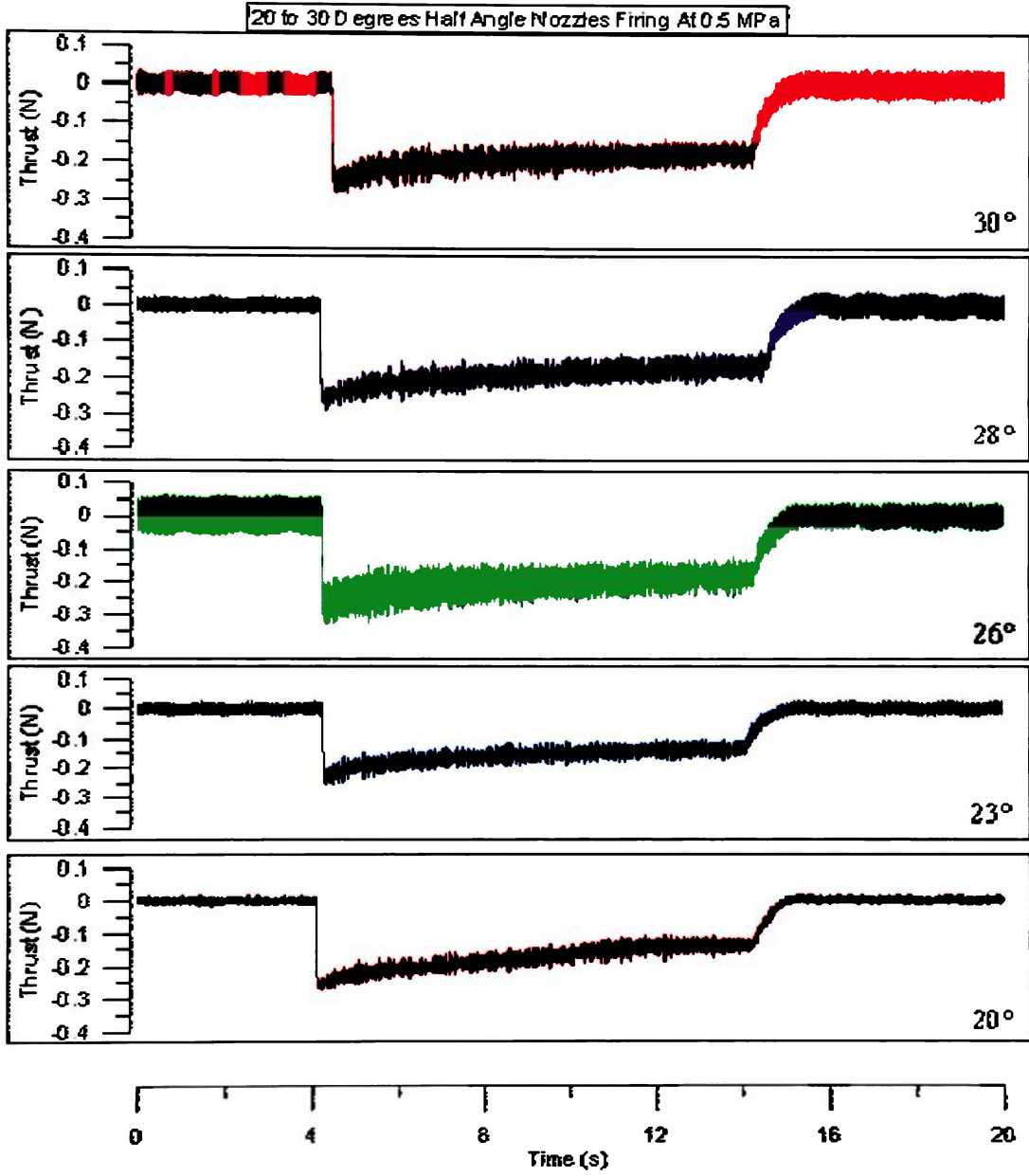


Figure A4. 20 to 30 degrees half angle nozzles firing at 0.5 MPa (vacuum).

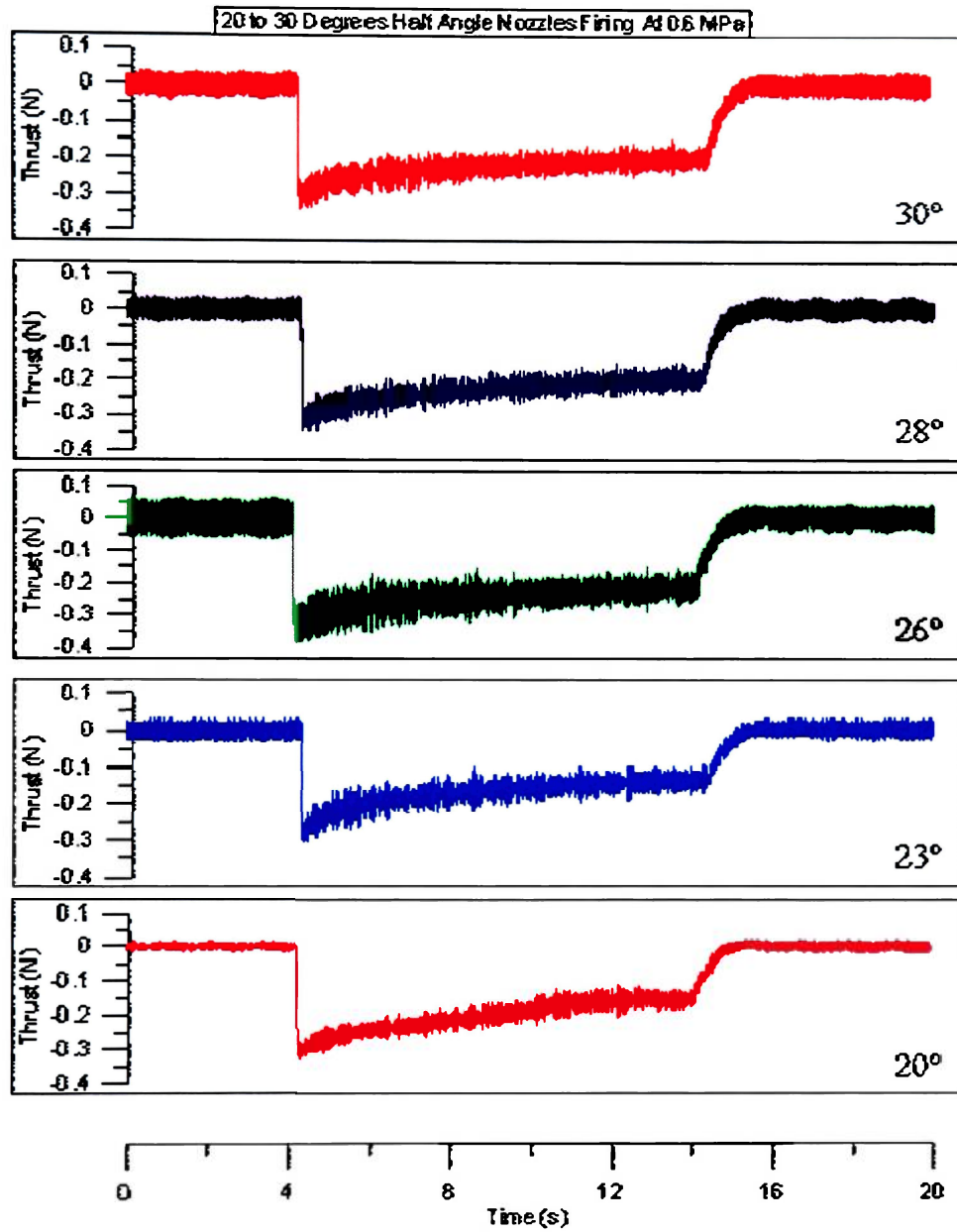


Figure A5. 20 to 30 degrees half angle nozzles firing at 0.6 MPa (vacuum).

Appendix B: Thrust Versus Pressure For Each Separate Nozzle Fired At Each Pressure (Vacuum Conditions)

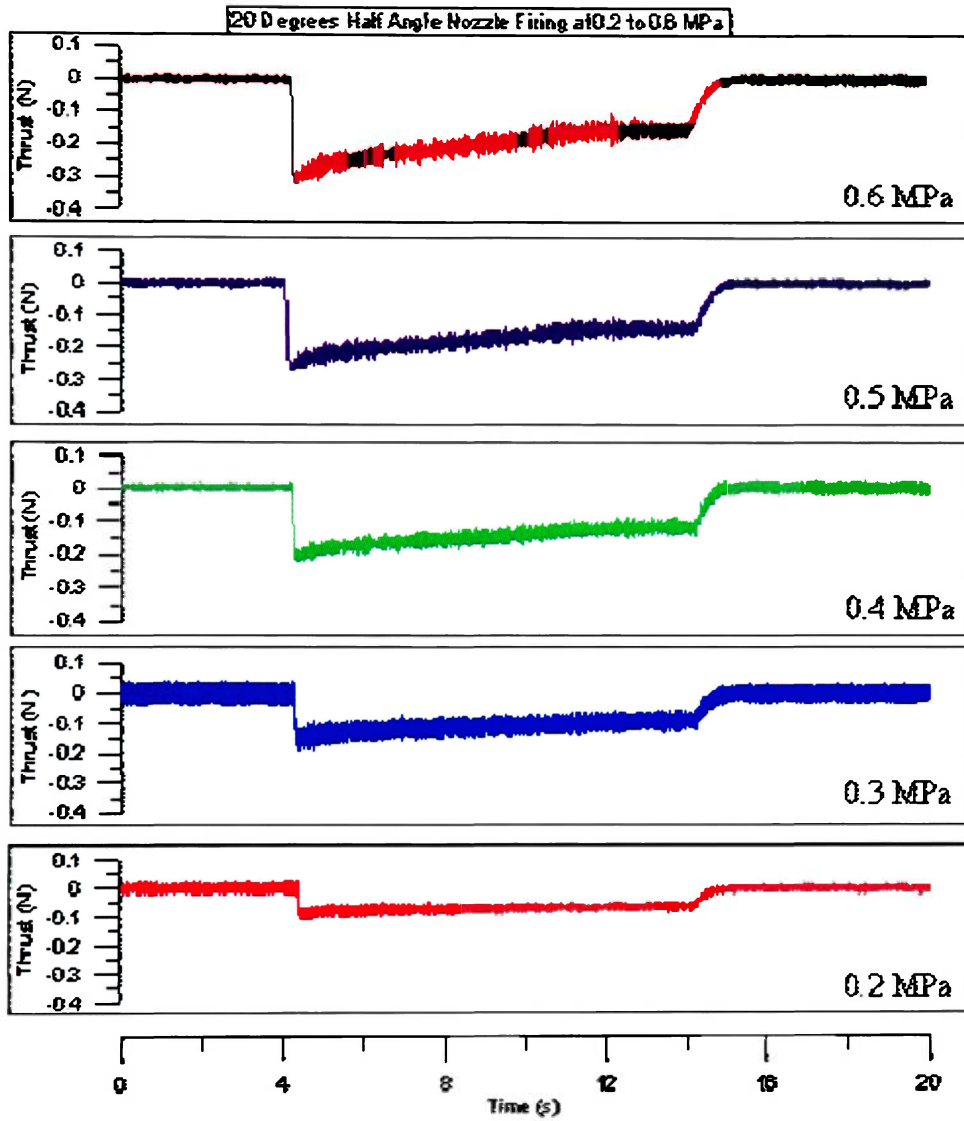


Figure A6. 20 degrees half angle nozzle firing at 0.2 to 0.6 MPa (vacuum).

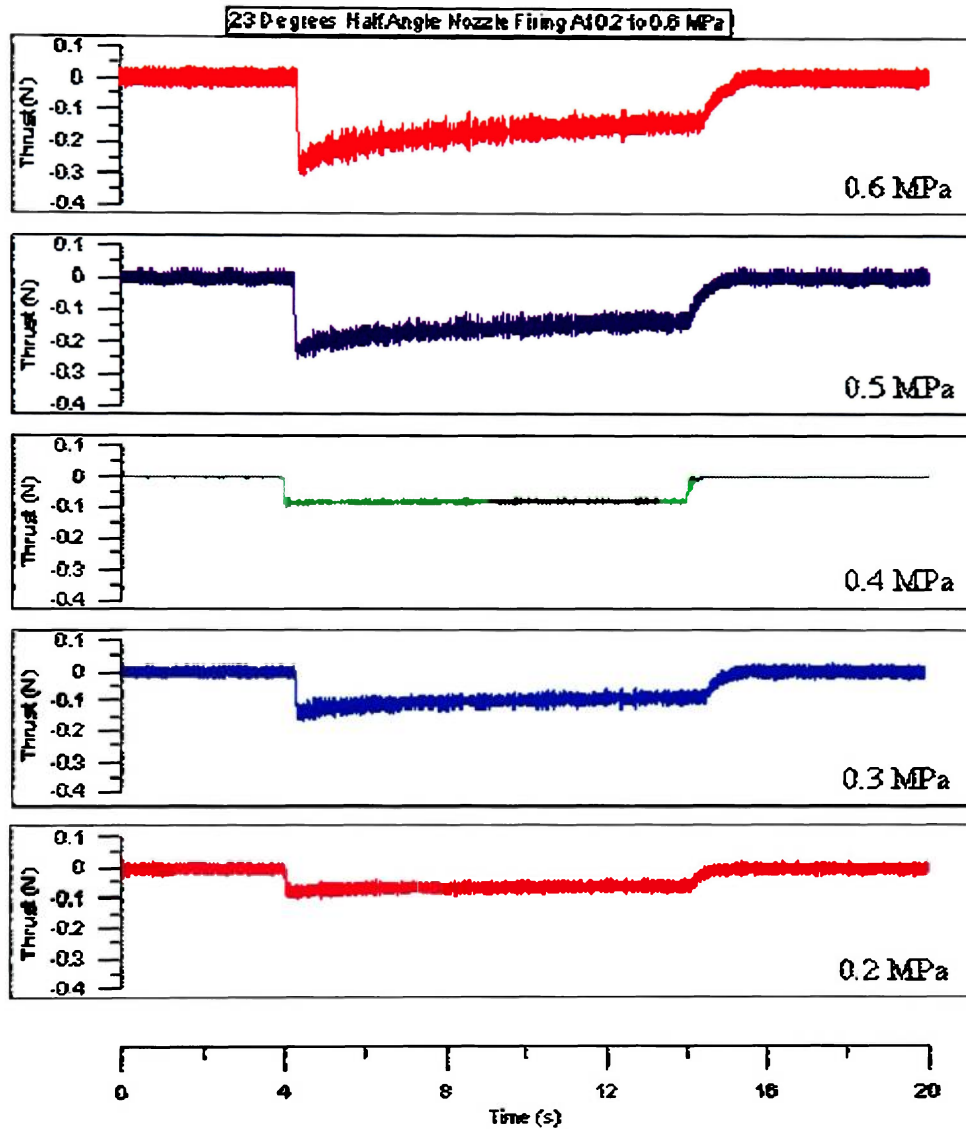


Figure A7. 23 degrees half angle nozzle firing at 0.2 to 0.6 MPa (vacuum).

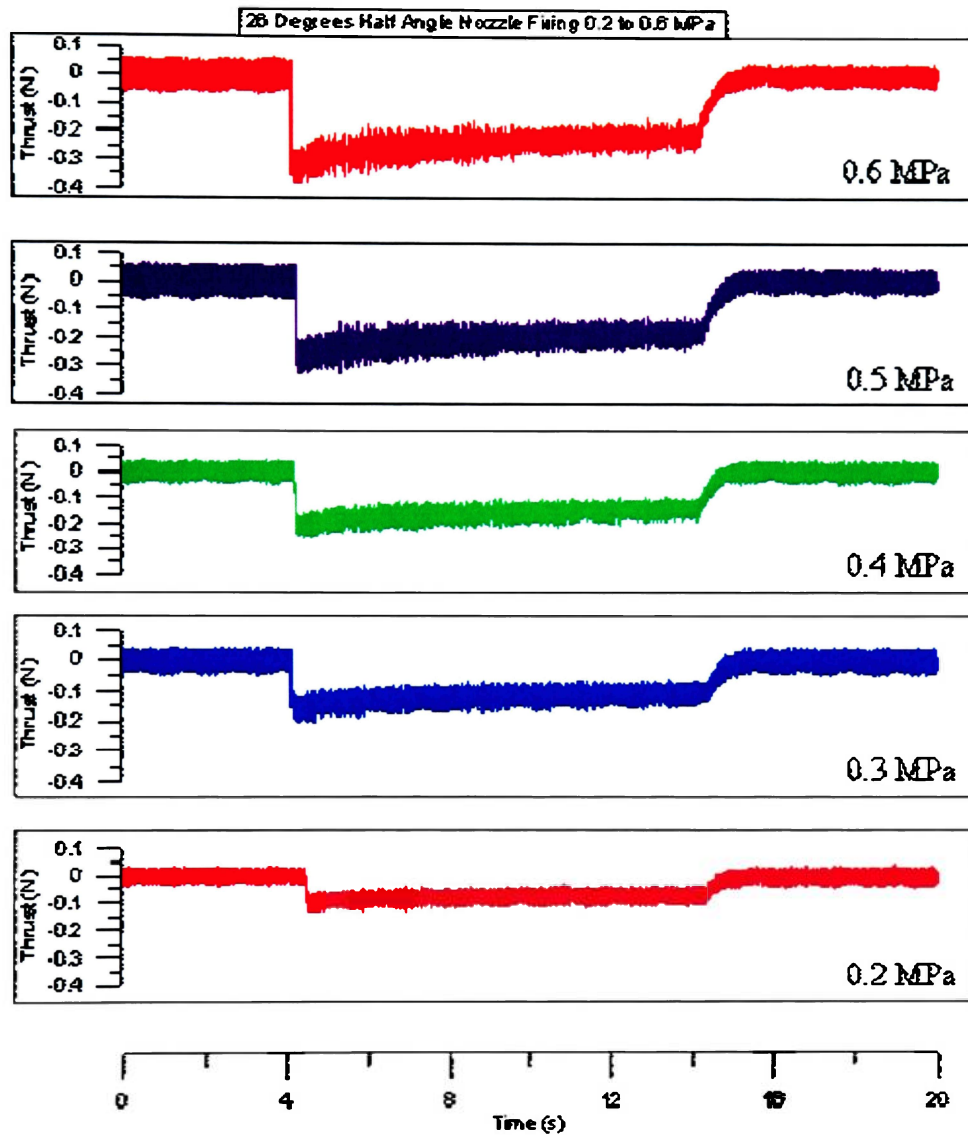


Figure A8. 26 degrees half angle nozzle firing at 0.2 to 0.6 MPa (vacuum).

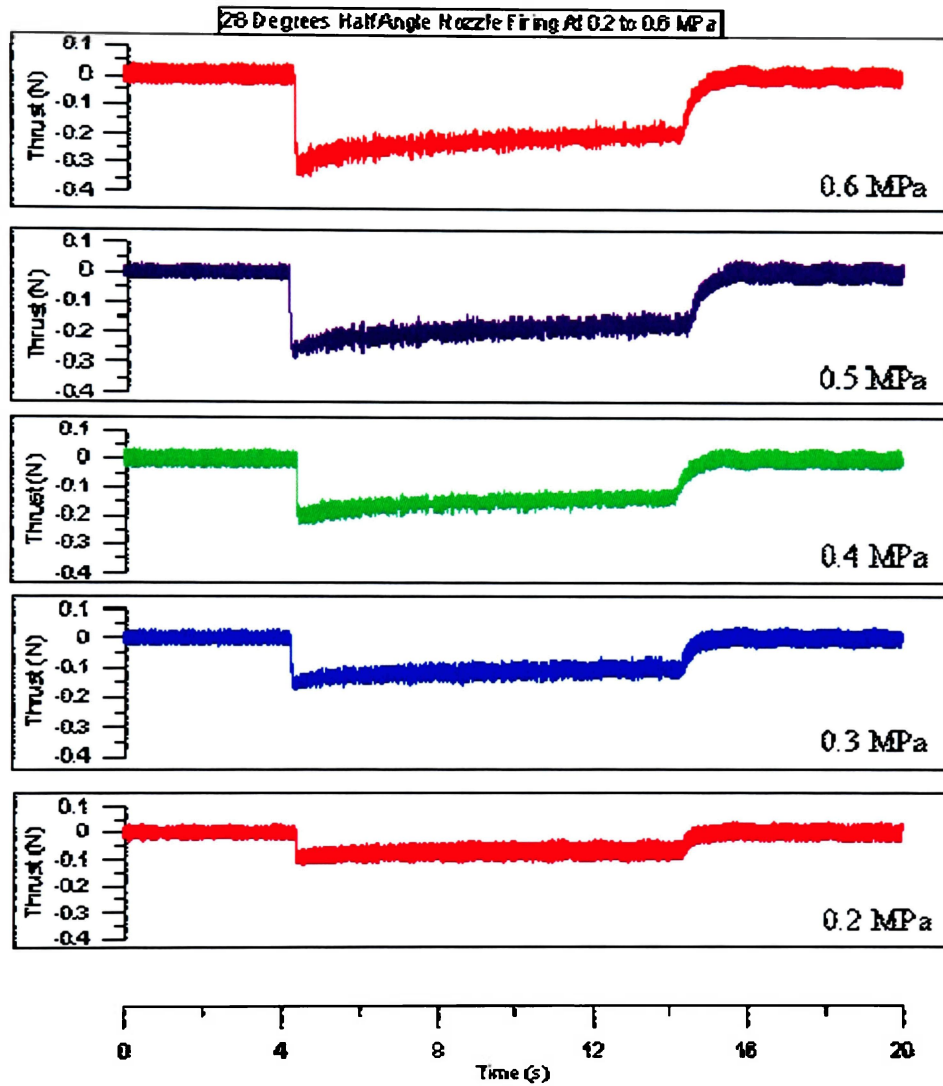


Figure A9. 28 degrees half angle nozzle firing at 0.2 to 0.6 MPa (vacuum).

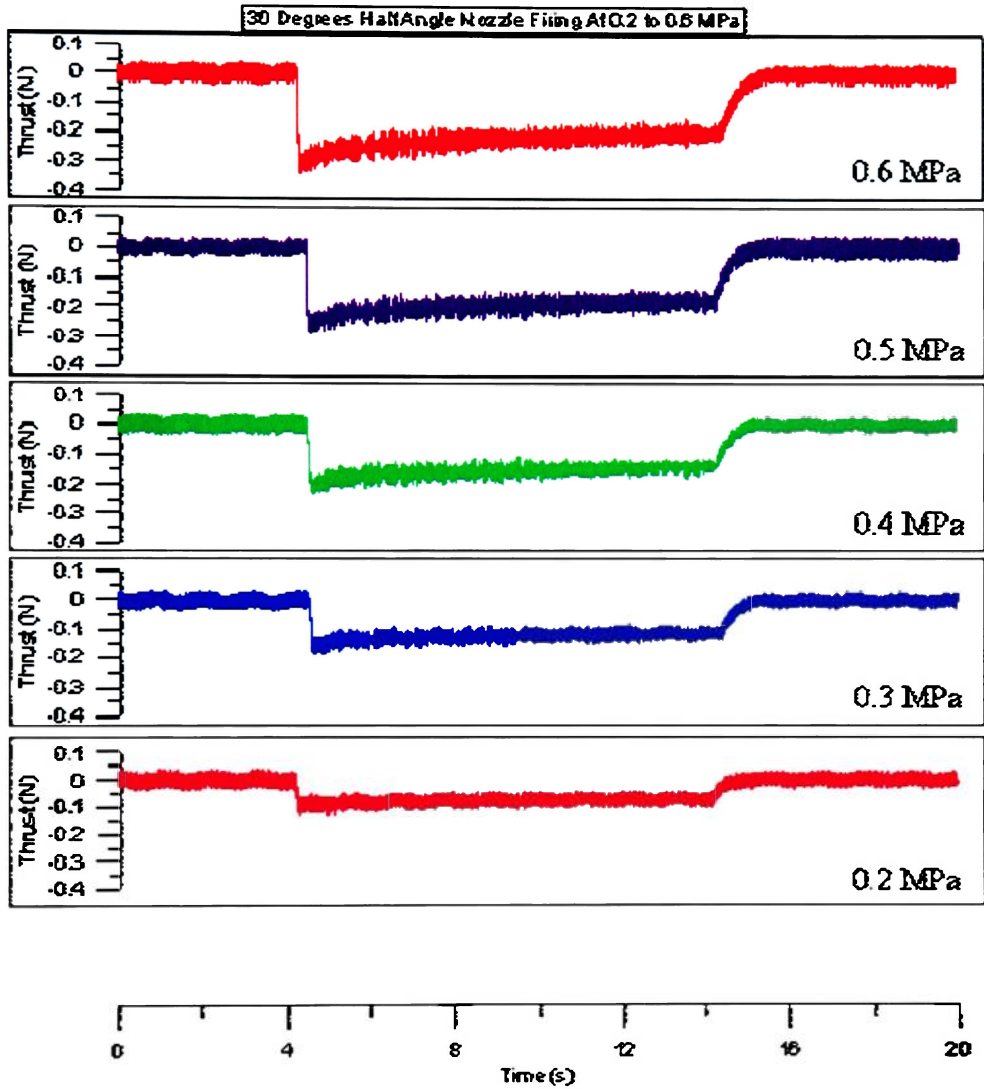


Figure A10. 30 degrees half angle nozzle firing at 0.2 to 0.6 MPa (vacuum).

Appendix C: Thrust Versus Pressure For All Five Nozzles Fired At The Same Pressure (Atmospheric Conditions)

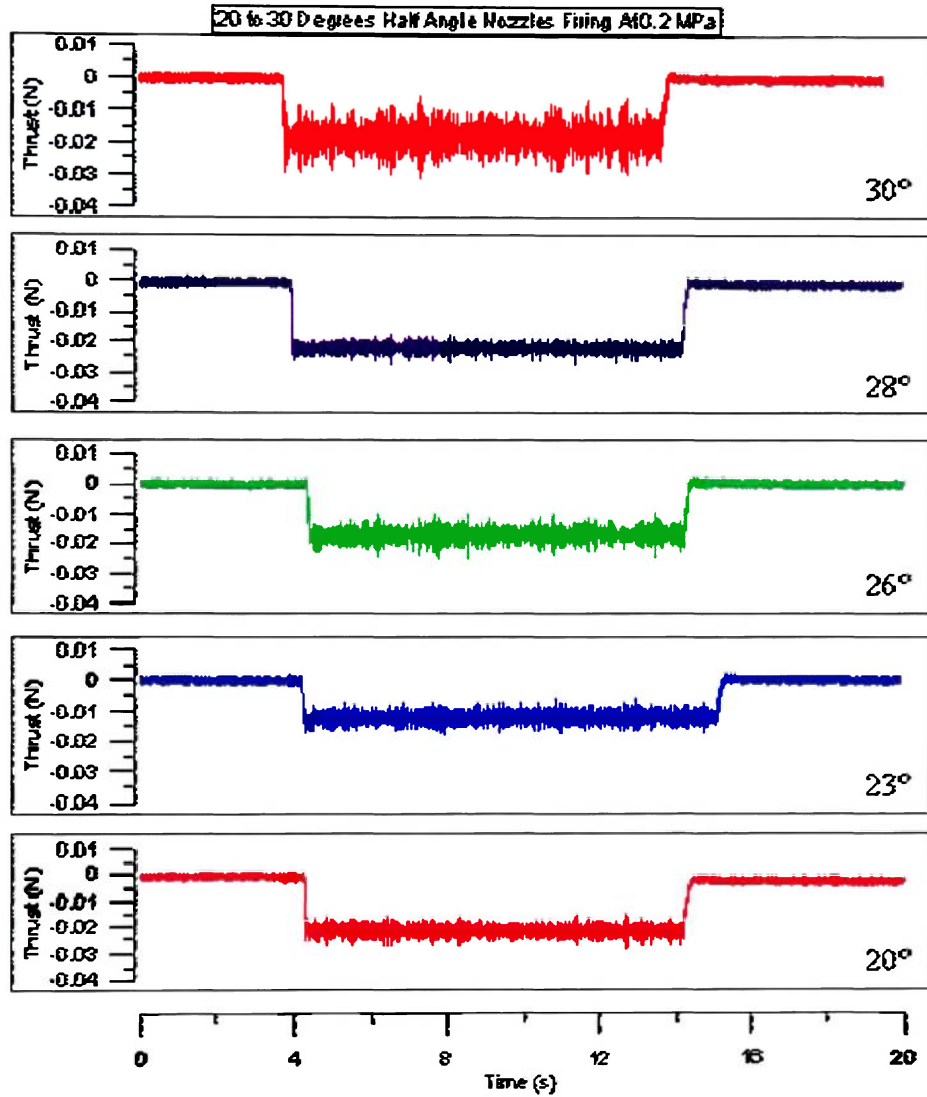


Figure A11. 20 to 30 degrees half angle nozzles firing at 0.2 MPa (atmosphere).

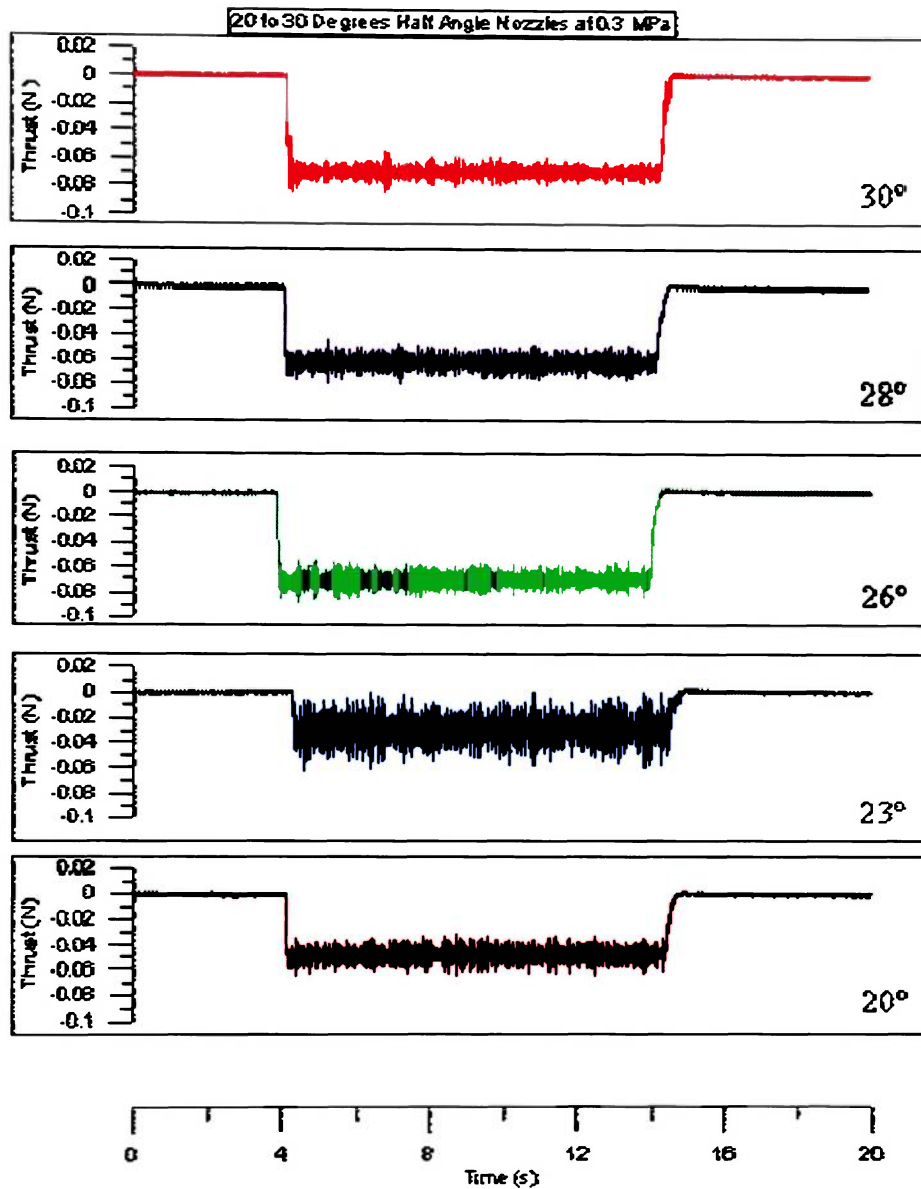


Figure A12. 20 to 30 degrees half angle nozzles firing at 0.3 MPa (atmosphere).

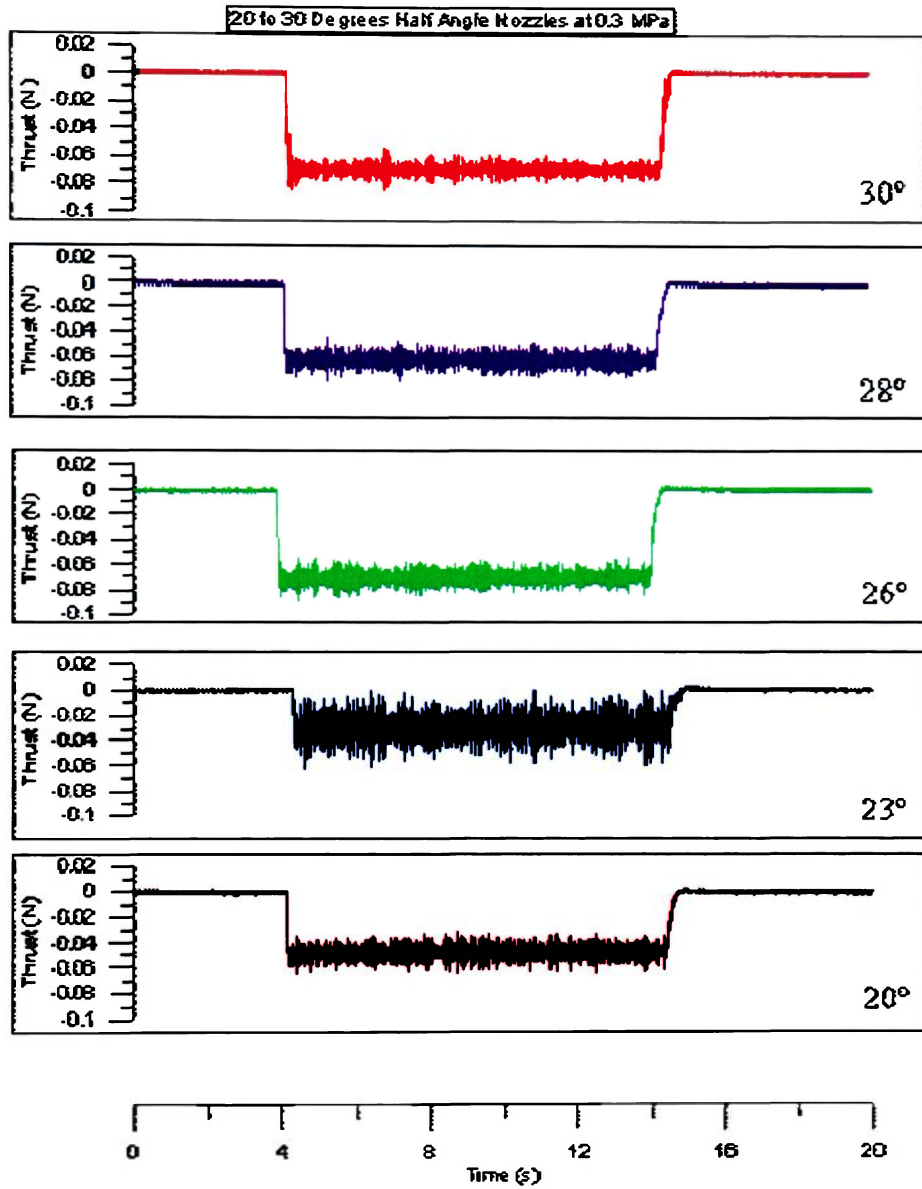


Figure A13. 20 to 30 degrees half angle nozzles firing at 0.4 MPa (atmosphere).

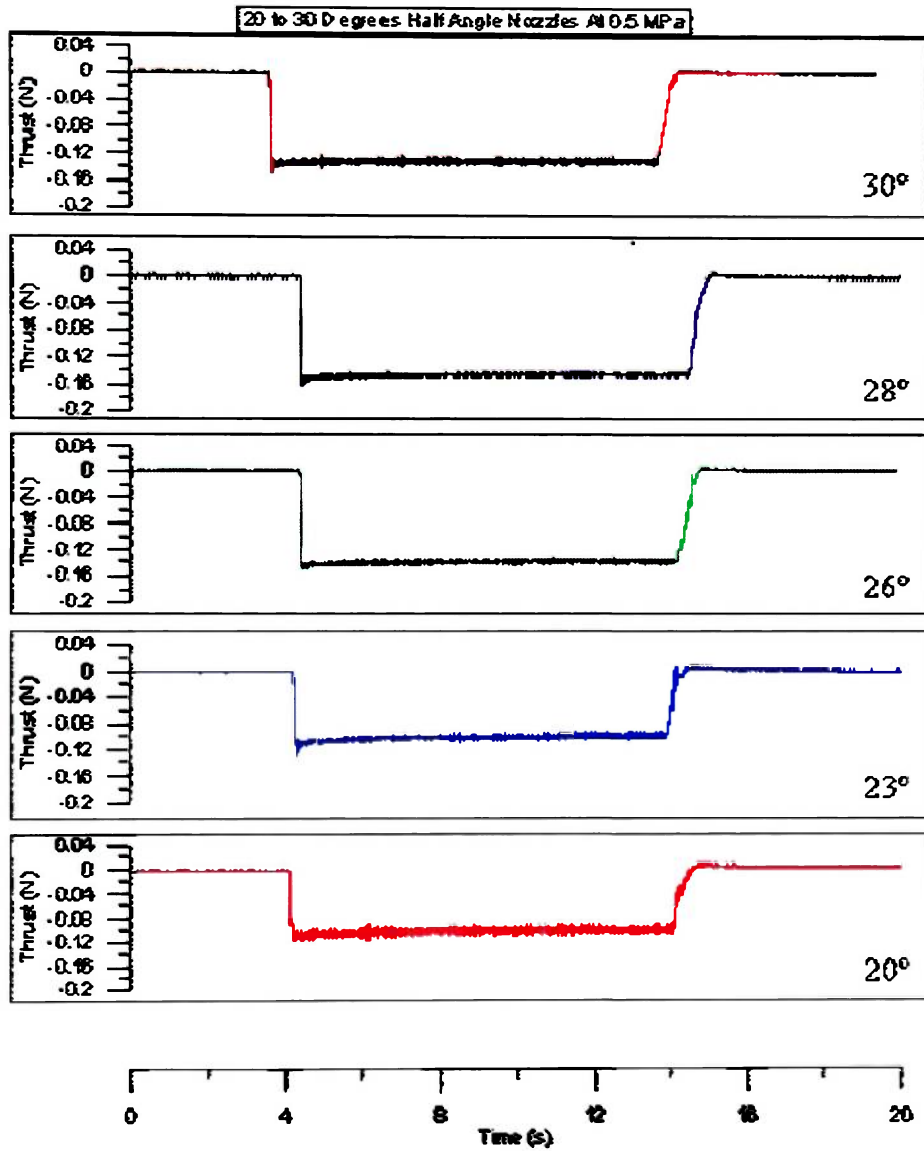


Figure A14. 20 to 30 degrees half angle nozzles firing at 0.5 MPa (atmosphere).

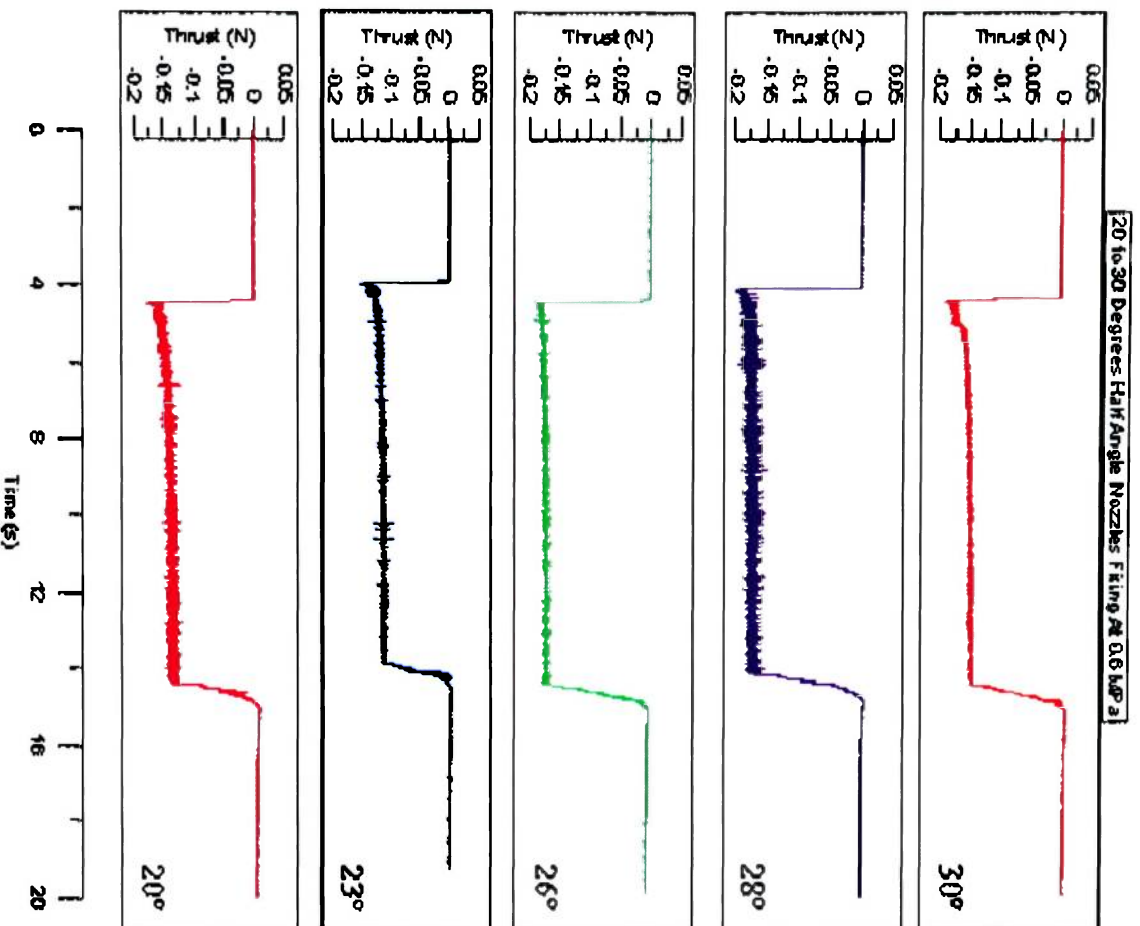


Figure A15. 20 to 30 degrees half angle nozzles firing at 0.6 MPa (atmosphere).

Appendix D: Thrust Versus Pressure For Each Separate Nozzle Fired At Each Pressure (Atmospheric Conditions)

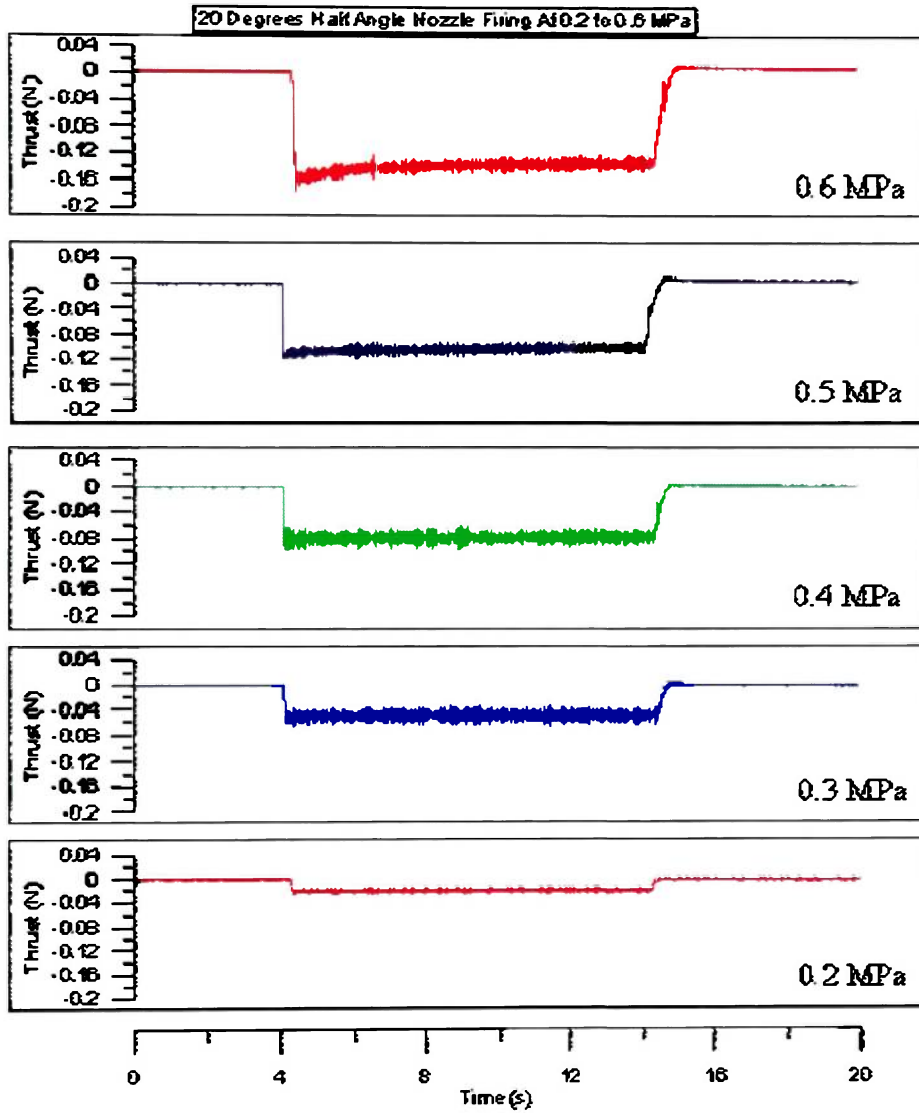


Figure A16. 20 degrees half angle nozzle firing at 0.2 to 0.6 MPa (atmosphere).

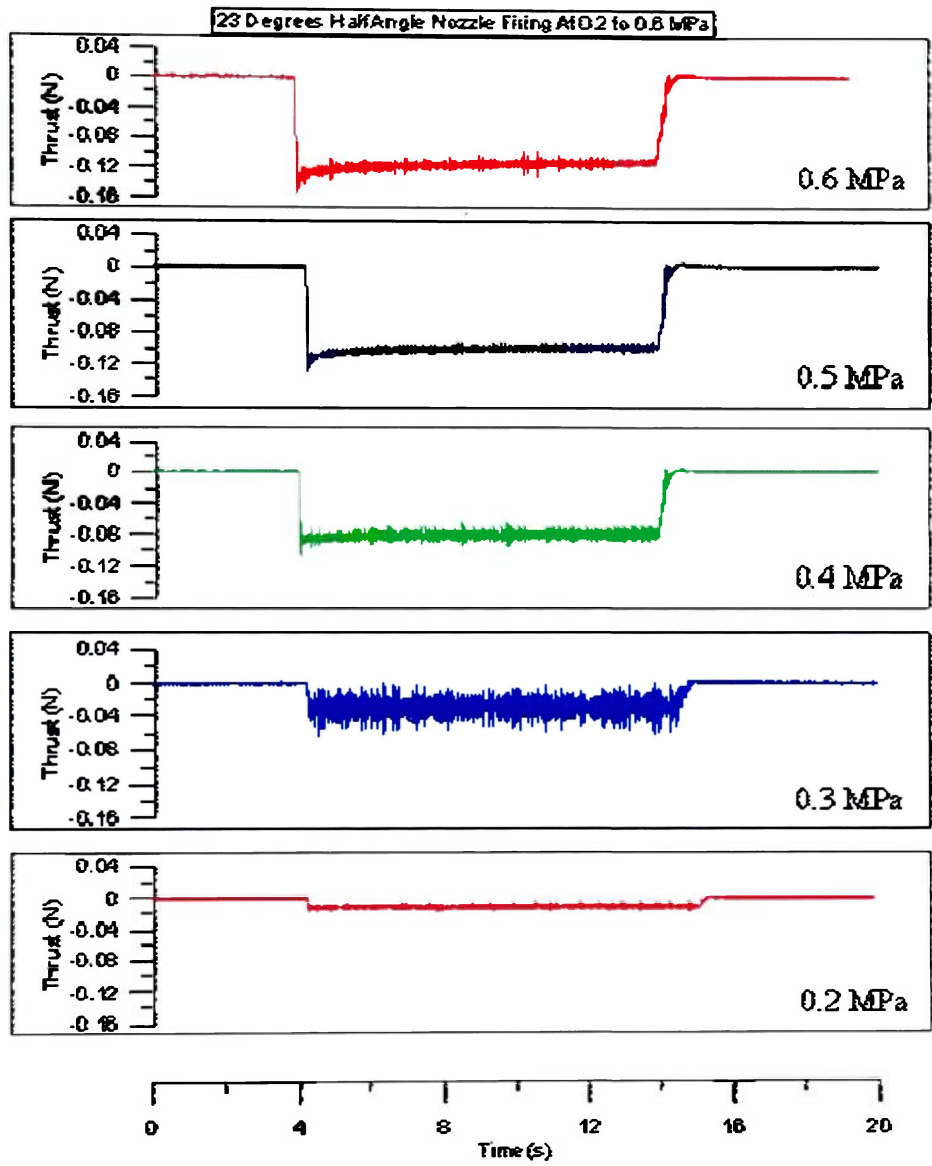


Figure A17. 23 degrees half angle nozzle firing at 0.2 to 0.6 MPa (atmosphere).

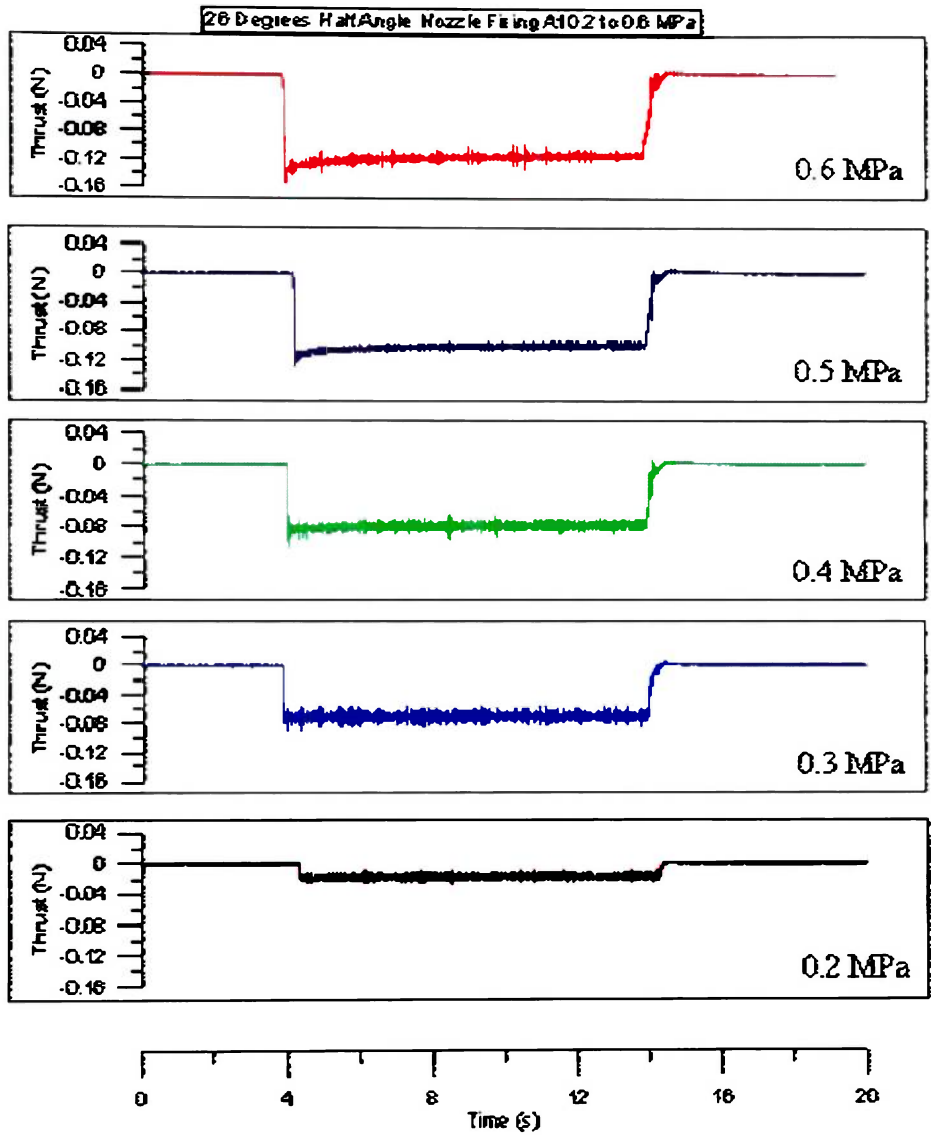


Figure A18. 26 degrees half angle nozzle firing at 0.2 to 0.6 MPa (atmosphere).

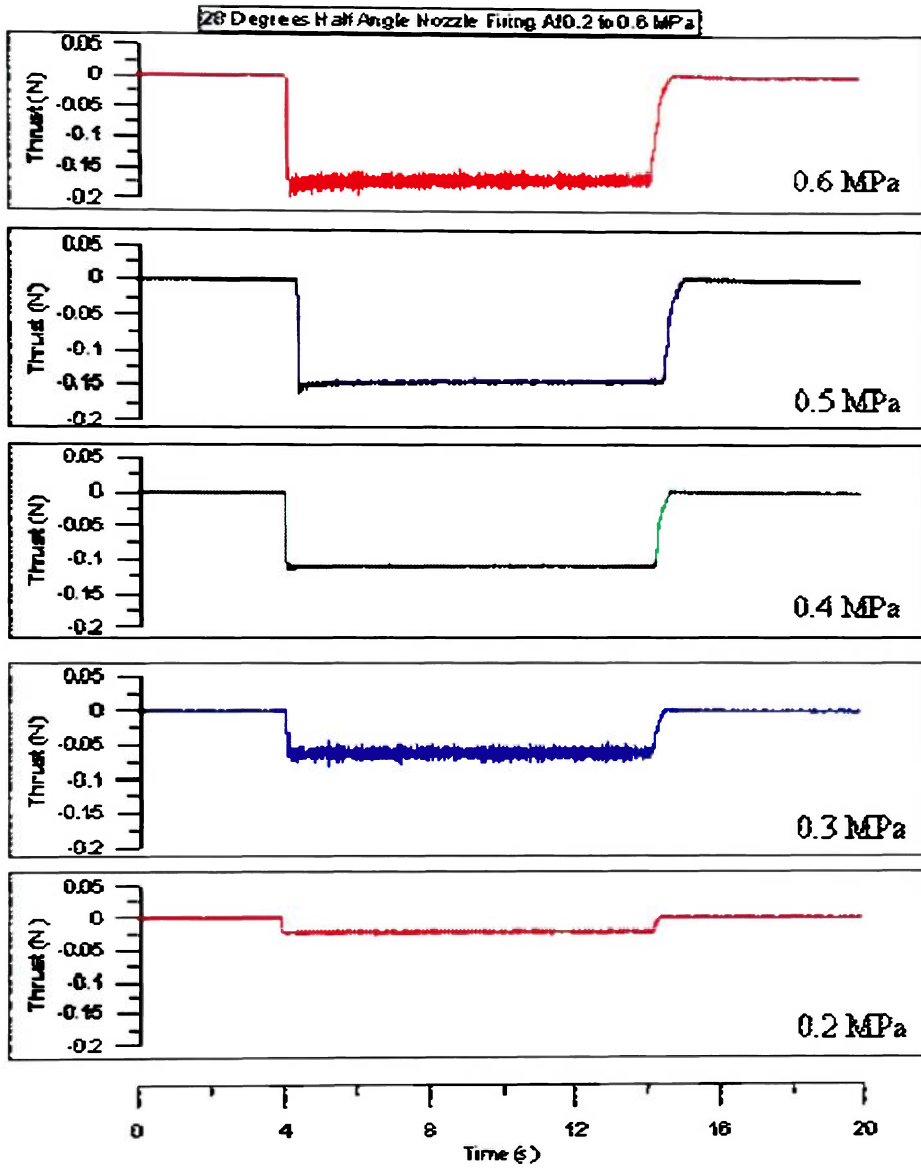


Figure A19. 28 degrees half angle nozzle firing at 0.2 to 0.6 MPa (atmosphere).

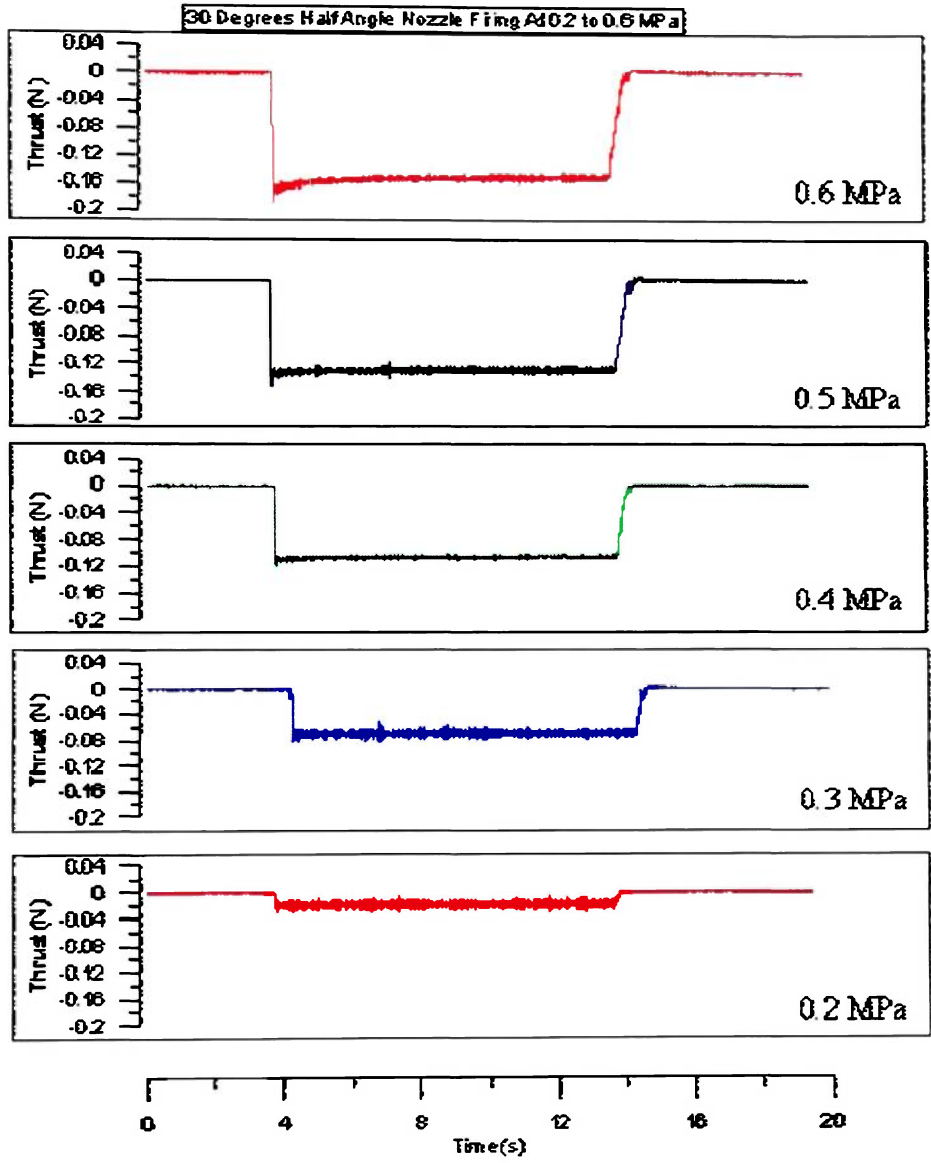


Figure A20. 30 degrees half angle nozzle firing at 0.2 to 0.6 MPa (atmosphere).